Development of highly accurate density functionals for H2 dissociation on transition metals

Smeets, E.W.F.

6 Performance of made-simple meta-GGA functionals with rVV10 non-local correlation for H_2 + Cu(111), D_2 + Ag(111), H_2 + Au(111) and D_2 + Pt(111)

This Chapter is based on:

Smeets, E. W. F.; Kroes, G.-J. Performance of made-simple meta-GGA functionals with rVV10 non-local correlation for H_2 + Cu(111), D_2 + Ag(111), H_2 + Au(111) and D_2 + Pt(111). *J. Phys. Chem. C* **2021**, DOI: 10.1021/acs.jpcc 0c11034

Abstract

Accurately modeling heterogeneous catalysis requires accurate descriptions of rate controlling elementary reactions of molecules on metal surfaces, but standard density functionals (DFs) are not accurate enough for this. The problem can be solved with the specific reaction parameter approach to density functional theory (SRP-DFT), but the transferability of SRP-DFs among chemically related systems is limited. We combine the MS-PBEl, MS-B86bl and MS-RPBEl semi-local made simple (MS) meta-GGA (mGGA) DFs with rVV10 non-local correlation, and we evaluate their performance for the hydrogen (H_2) + Cu(111), deuterium (D_2) + Ag(111), H_2 + Au(111) and D_2 + Pt(111) gas-surface systems. The three MS mGGA DFs that have been combined with rVV10 non-local correlation were not fitted to reproduce particular experiments, nor has the b parameter present in rVV10 been re-optimized. Of the three DFs obtained the MS-PBEl-rVV10 DF yields an excellent description of van der Waals well geometries. The three original MS mGGA DFs gave a highly accurate description of the metals, which was comparable in quality to that

obtained with the PBEsol DF. Here we find that combining the three original MS mGGA DFs with rVV10 non-local correlation comes at the cost of a slightly less accurate description of the metal. However the description of the metal obtained in this way is still better than the descriptions obtained with SRP-DFs specifically optimized for individual systems. Using the Born-Oppenheimer static surface (BOSS) model simulations of molecular beam dissociative chemisorption experiments yields chemical accuracy for the D_2 + Ag(111) and D_2 + Pt(111) systems. A comparison between calculated and measured $E_{1/2}(\nu, J)$ parameters describing associative desorption suggest chemical accuracy for the associative desorption of H_2 from Au(111) as well. Our results suggest that ascending Jacob's ladder to the mGGA rung yields increasingly more accurate results for gas-surface reactions of H_2 (D_2) interacting with late transition metals.

6.1 Introduction

In heterogeneous catalysis the rate-limiting step is often the dissociative chemisorption of a molecule on a surface[2,3]. The dissociation of the simple hydrogen (H_2) and nitrogen (N_2) molecules are important steps in the production of ammonia and syngas[4–6]. The dissociation of H_2 is also relevant to the industrial synthesis of methanol from CO_2 over a $Cu/ZnO/Al_2O_3$ catalyst, for which the dissociation of H_2 is considered to be a rate-limiting step[7–9]. Calculating chemically accurate barrier heights[10] for rate-controlling reactions to obtain accurate rates of the overall reaction network[11] potentially has a large financial impact on the chemical industry since it allows theoretical screening for more efficient catalysts[12].

Currently density functional theory (DFT) is the only method that is computationally cheap enough to map out full potential energy surfaces (PESs) for gas-surface reactions. Development of density functionals (DFs) that can accurately describe dissociative chemisorption reactions on surfaces is important to increasing the predictive power of DFT. DFs constructed using the generalized gradient approximation (GGA) that provide chemically accurate results for specific gas-surface reactions and that in some cases show transferability to chemically related systems are based on the semi-empirical specific reaction parameter (SRP) approach to DFT (SRP-DFT)[13–16]. However, DFs at the GGA level are always a compromise between a good description of the molecule and of the metal[17], despite efforts to construct GGA based DFs[18] or non-separable gradient approximation DFs[19] that perform equally well for both solids and molecules. A good description of the metal is crucial to calculating accurate barrier heights since the barrier height might depend on the interlayer distance

of the two top most metal layers[20–22] and the amplitude of thermal motion of the metal atoms in the top layer[23,24].

In Chapter 3 we developed the semi-local MS-PBEl, MS-B86bl and MS-RPBEl meta-GGA (mGGA) DFs[25] based on the made simple (MS) formalism[26,27], which yield a description of the metal that is similar in accuracy to that obtained with the PBEsol[28] DF. Additionally the DFs provide a chemically accurate description of molecular beam experiments on dissociative chemisorption of H_2 (D_2) on Cu(111)[25,29–31] and a near chemically accurate description of similar experiments on D_2 + Ag(111)[25,32]. The reason behind this improved overal performance of mGGA based DFs over GGA based DFs is that mGGA DFs also depend on the kinetic energy density τ, which allows a DF to distinguish between regions of the electron density describing single (covalent), metallic, and weak bonds[33] via the dimensionless inhomogeneity parameter α[26,27,33]. This parameter has also been used in the construction of several other much used mGGA DFs, such as TPSS[34], revTPSS[35], RTPSS[36], SCAN[37,38] and mBEEF[39]. Several groups have now reported good simultaneous descriptions of lattice constants and adsorption energies[39–41], or, more generally, energetics and structure[26,27,42,43], when using mGGA DFs. The MS-RPBEl DF has also shown some success in describing the O_2 + Al(111) system[16].

In Chapter 5 we also identified non-local correlation as a key ingredient for a DF that can describe dissociative chemisorption of H_2 (D_2) with chemical accuracy on multiple metals[15] and not just on different crystal faces of the same metal[44,45], which had previously only been demonstrated for reactions of CH_4 with metal surfaces, i.e. Ni(111)[46] and Pt(111)[47]. Here we combine the three previously developed MS mGGA DFs with rVV10[48] non-local correlation in order to obtain the MS-PBEl-rVV10, MS-B86bl-rVV10 and MS-RPBEl-rVV10 DFs, and we will evaluate their performance for the H_2 + Cu(111), Ag(111), Au(111) and Pt(111) systems. The three original MS mGGA DFs[25] which we combine with rVV10[48] non-local correlation show no van der Waals interactions for H_2 interacting with transition metals[15], which is the best case scenario to complement a semi-local exchange-correlation functional with (r)VV10 non-local correlation according to Vydrov et al.[49].

The PESs we computed with the three new DFs are subsequently used in quasi-classical trajectory (QCT) calculations. In the dynamics calculations we use the Born-Oppenheimer static surface (BOSS) model, which is known to work well for activated H_2 dissociation on cold metals[50–54]. Calculations that incorporate surface motion show that the impact of surface atom motion (phonons) can be neglected due to the effect on the reaction probability being small for the low surface temperature experiments considered here[20,22,52,55]. It is also justified to neglect the effect of electron-hole pair excitation on the reaction

probability, as its effect on sticking has previously been shown to be small in calculations on H_2 + Cu(111)[56–58], Ag(111)[59–61], and Ru(0001)[62]. Previous research has also shown that for highly activated dissociation of H_2 on cold metals the difference between quantum dynamics (QD) and QCT calculations is marginal[15,63,64] (see also Chapter 4), and there is also some evidence that the same observation holds for the non-activated reaction of D_2 + Pt(111) for all but the lowest translational energies[14,65]. Since our dynamical model is best suited to molecular beam dissociative chemisorption experiments, we will mainly compare to this kind of experiment[29–32,66,67] to assess the quality of the obtained DFs. These experiments have been performed for H_2 + Cu(111)[29–31], Ag(111)[32] and Pt(111)[66–68].

Additionally we will also compare to the associative desorption experiments that are available for the H_2 (D_2) + Au(111)[69] and Ag(111)[70,71] systems as in Chapter 5, by comparing the measured $E_0(\nu, J)$ parameters characterizing the measurements with calculated $E_{1/2}(\nu, J)$ parameters[15] assuming detailed balance. Given that the DFs developed here are too reactive with respect to the H_2 (D_2) + Cu(111) system (as will be shown below) we will omit such an analysis for the recent associative desorption experiments[72] for this system here. For the H_2 + Cu(111) system it is known that the effect of surface motion cannot readily be ignored for specific observables at high surface temperature[53] (T_s), and this may hold for the H_2 + Au(111) and Ag(111) systems as well. Therefore it is difficult to assess the quality of the developed DFs when using the BOSS model in comparing to high surface temperature experiments[69,72], as will be done below. We note that it is also possible to simulate associative desorption directly by running trajectories starting around the transition state using Metropolis sampling of the initial conditions[73–77], and that this has also been done for H_2 and D_2 desorbing from Cu(111). There are some limitations regarding these calculations: in earlier work[74,75] a PES that is an approximate fit[78] to unconverged DFT calculations[79] was used. The statistical accuracy of the later work[77] is limited by the number of ab initio molecular dynamics (AIMD) trajectories that have been calculated.

The van der Waals well geometries obtained from our DFT calculations will be compared to experimental results, which are mostly obtained from analysis of selective adsorption experiments[80–90]. In these experiments, an increase or a dip is observed in a peak associated with a rotational (rotationally mediated selective adsorption, RMSA[80]) transition or in a peak for a diffractive (corrugation mediated selective adsorption, CMSA[91,92]) transition if the translational energy passes through a value that overlaps with the energy difference between two hindered rotational or parallel translational metastable states, respectively. The H_2 molecule is then trapped in the final state in the van der Waals well close

to the surface[82,87]. The resonance energies can then be used to reconstruct the shape of the potential and thus to determine the van der Waals well depths and geometries. Concerning the systems investigated here, studies using experiments to analyze the van der Waals interaction have been performed for H_2 + Cu(111)[89,90], Ag(111)[83,84,86], Au(111)[90], and Pt(111)[80–82,93].

6.2 Methodology

6.2.1 Coordinate system

In the dynamics calculations we use the BOSS model[13], meaning that we make the Born-Oppenheimer approximation and keep the surface atoms fixed at their ideal lattice positions. We only take into account the six degrees of freedom (DOF) of the H_2 molecule (see figure 6.1a). We use molecular coordinates in which the center of mass (COM) coordinates X, Y describe the lateral position of the molecule, and Z describes the molecule surface distance. The remaining DOFs are the H_2 bond length r, the polar angle θ and the azimuth ϕ defining the orientation of the molecule relative to the surface (see figure 6.1a). The geometry of the (111) face of an fcc metal together with its high symmetry sites is shown in relation to the coordinate system used in figure 6.1b.

6.2.2 Combining Made Simple meta-GGA exhcange-correlation with rVV10 non-local correlation

The form of the rVV10[48] non-local correlation functional is similar to that of the Rutgers-Chalmers vdW-DFs[38]:

$$E_c^{\text{non-local}} = \int d\boldsymbol{r} n(\boldsymbol{r}) \Big(\frac{\hbar}{2} \int d\boldsymbol{r}' \Phi(\boldsymbol{r}, \boldsymbol{r}') n(\boldsymbol{r}') + \beta \Big). \tag{6.1}$$

Here $n(\boldsymbol{r})$ is the electron density and $\Phi(\boldsymbol{r}, \boldsymbol{r}')$ is the kernel describing the density-density interactions[38]. The parameter β is not present in the vdW-DF1[94] and vdW-DF2[95] non-local correlation functionals and is here taken to be $\beta = \frac{1}{32}(\frac{3}{b})^{\frac{3}{4}}$ so as to ensure that $E_c^{\text{non-local}}$ is zero for the homogeneous electron gas[38]. In using the full exchange-correlation functional named rVV10, most researchers we are aware of[38,96,97] now append the non-local correlation (NLC) rVV10 functional to the following semi-local functional (SLF)

$$E_{xc}^{VV10-SL} = E_x^{rPW86} + E_c^{PBE}. \tag{6.2}$$

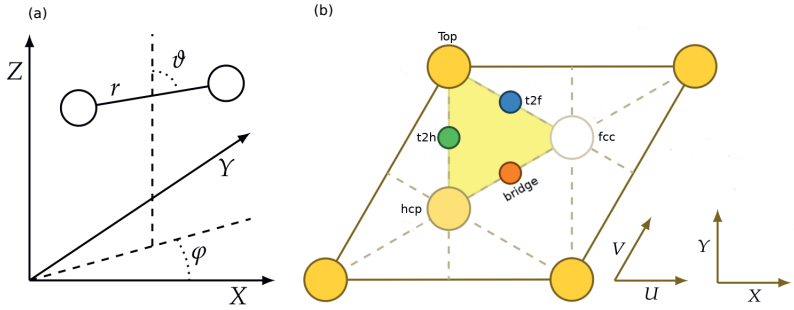

FIGURE 6.1: The COM coordinate system used for the description of the H_2 (D_2) molecule (a). The unit cell of a (111) face of a fcc metal together with the high symmetry sites as well as the relationship with the coordinate system chosen for H_2 (D_2) relative to the (111) surface (b). The origin of the COM coordinate system $(X, Y, Z) = (0, 0, 0)$ is the center of a top atom. We define the polar angle and azimuth such that $(\theta = 90°, \phi = 0°)$ corresponds to molecules parallel to the surface pointing along the X (or equivalent U) direction. The hcp and fcc hollow sites correspond to metal atoms in the second and third layer. Note that the colored triangle marks the irreducible wedge of the (111) unit cell.

Here, E_x^{rPW86} is the exchange part of a refitted version of the PW86 functional[98], and E_c^{PBE} is the PBE correlation functional[99]. In implementing the full rVV10 functional, DFT codes like Quantum Espresso[100,101] and Q-Chem[102] also append the NLC functional defined by Eq. 6.1 to the SLF defined by Eq. 6.2. Eq. 6.2 also defines the semi-local exchange correlation functional to which Vydrov et al.[49] appended their NLC VV10 functional to in order to obtain the full exchange correlation functional now referred to as the VV10 functional. Sabatini et al.[48] obtained the NLC rVV10 functional of (Eq. 6.1) by making a minor change to the NLC VV10 functional[49] in a clever way to make it amenable to efficient evaluation by the algorithm due to Róman-Pérez and Soler[103] that can also be used to speed up the evaluation of the vdW-DF1 and vdW-DF2 density functionals of the Lundqvist-Langreth group[94,95]. To reproduce the original VV10 results as closely as possible, Sabatini et al.[48] changed one of the empirical parameters in the NLC rVV10 functional, i.e., the b-parameter, from the original VV10 value of 5.96 to the rVV10 value of 6.37. Here, the b parameter can be used to control the damping of the kernel at short range, while the other empirical parameter in VV10 and rVV10, C, can be used to obtain good values for the C_6 dispersion coefficients describing the long-range van der Waals interaction. The C parameter is taken the same[48] in the NLC rVV10 as in the NLC VV10 functional[49].

We note that there is some ambiguity associated with the SLF Sabatini et al.[48] originally appended their NLC rVV10 functional to. In a sentence saying that they were "following the original VV10 functional definition", they provided an equation for the full rVV10 functional in which the SLF to which the NLC rVV10 functional was appended would be given by

$$E_{xc}^{vdW-DF2} = E_x^{rPW86} + E_c^{LDA}. \tag{6.3}$$

The equation they presented suggested that in their SLF PBE correlation was replaced with correlation from the local density approximation (where Sabatini et al.[48] state they used the functional as parameterized by Perdew and Wang[104]). This SLF happens to be the same as the one used with the non-local vdW-DF2 functional to obtain the full vdW-DF2 functional[95]. Regarding the SLF originally used, we think the equation provided by Sabatini et al.[48] contained a misprint, and that they in fact used the expression of Eq. 6.2 instead. Our reason for stating this is that the energies they present for the S22 database[105] in Table 1 of their Supporting material to Ref.[48], which they computed with their rVV10 functional but using the b parameter from the original VV10 functional, were in excellent agreement with the original VV10 results computed by Vydrov et al.[49]. We believe that this would not have been

the case had Sabatini et al.[48] used Eq. 6.3 as Vydrov et al.[49] certainly used Eq. 6.2; the difference between the PBE and LDA semi-local contributions should have been too large to allow for the small differences obtained between the rVV10 with $b = 5.9$ and VV10 results that were obtained in practice[48]. Even more importantly, the rVV10 results obtained by Peng et al.[38], who used Eq. 2 for the SLF, for the S22 database[105] as provided in table 4 of their paper[38] closely reproduce the rVV10 results of Sabatini et al.[48] as provided in table 1 of their supporting material[48]. Once, again, this would not have been the case had these teams used different SLFs appended to the NLF rVV10 DF.

More importantly to the purpose of the present work than the exact expression of the full rVV10 functional, the flexibility built in to the NLC rVV10 functional through the adjustable b parameter allows it to be used in combination with a number of exchange-correlation functionals, including mGGA functionals like the SCAN functional[37] and the B97M functional incorporated into the B97M-rV functional[97]. It is in this context that we use the NLC rVV10 functional, hoping that in this way we can obtain a good description of the long-range interaction, while hopefully keeping the medium-range interaction, which we think is reasonably described with the mGGA functionals[25] we will be testing as SLFs, intact, in the spirit of Peng et al.[38]. In this Chapter, the full exchange-correlation functional then takes the following form:

$$E_{xc}^{\text{MS-mGGA-rVV10}} = E_x^{\text{MS-mGGA}} + E_c^{\text{revTPSS}} + E_c^{\text{rVV10}}, \tag{6.4}$$

where E_c^{revTPSS} is the revTPSS[35] correlation functional that is used in the original semi-local MS mGGA DFs we developed[25]. $E_x^{\text{MS-mGGA}}$ can be either of the three MS mGGA exchange functionals we developed previously[25] based on the MS formalism[26]. In this formalism one interpolates between two GGAs for two extreme scenarios, namely a single orbital system which describes covalent bonds ($F_x^0(p;c)$) and one in which the bonding is metallic ($F_x^1(p)$)[25]. The exchange enhancement factor of a MS mGGA DF then becomes[26]:

$$F_x^{\text{MS}}(p,\alpha) = F_x^1(p) + f(\alpha)(F_x^0(p;c) - F_x^1(p)), \tag{6.5}$$

where $p = s^2$ with s being the reduced gradient of the electron density[26], and $F_x^1(p)$ and $F_x^0(p;c)$ are gradient enhancement factors that depend solely on p. The numerical parameter c is optimized to exactly reproduce the exchange energy of the hydrogen atom by cancelling the spurious self-interaction present in the Hartree energy in this atom[26]. For both $F_x^1(p)$ and $F_x^0(p;c)$ three expressions[25] have been used which are PBE-like[99], RPBE-like[106] and B86b-like[107], in the sense that we use the gradient enhancement expression of the PBE[99], RPBE[106] and B86b[107] GGA DFs but with $\mu = \frac{10}{81}$ as was done in

PBEsol[28]. The difference between $F_x^1(p)$ and $F_x^0(p;c)$ is that in the case of $F_x^0(p;c)$ we replace μp by $\mu p + c$ everywhere[25], as done earlier in ref[26]. The interpolation between the two extreme cases then happens through a function of the inhomogeneity parameter $f(\alpha)$, with the inhomogeneity parameter being defined as:[26,27]

$$\alpha = \frac{\tau - \tau^W}{\tau^{\text{unif}}}. \tag{6.6}$$

Here, τ^W is the Von Weizäcker kinetic energy, which is equal to the kinetic energy density associated with a single orbital electron density[41], and τ^{unif} is the kinetic energy of the homogeneous electron gas. Note that α will approach unity as $\tau \approx \tau^{\text{unif}}$ and $\tau^W \ll \tau^{\text{unif}}$ for slowly varying electron densities, while α approaches zero for densities found in covalent bonding for which $\tau \approx \tau^W$[41]. The expression for $f(\alpha)$ can be found in Refs.[25,26].

Above, we have already noted that the possibility to adapt the b parameter allows for flexibility in the combination of the NLC rVV10 functional with SLFs. In the past several strategies have been used to arrive at a good choice of b. In perhaps the most rigorous approach, in the original papers presenting the full VV10[49] and rVV10[48] functionals the b parameter was chosen to minimize the errors in the binding energies of weakly bonded dimers as present in the S22 database[105]. In a simplified procedure requiring fewer calculations, the b parameter has also been determined by demanding that calculations with the NLC rVV10 functional reproduce the Ar dimer energy curve determined with CCSD(T) calculations[97] as closely as possible[38,48,96,97]. In the development of functionals for specific purposes, the b parameter has also been fitted to more specific properties corresponding to these purposes. For instance, functionals have been developed that give good descriptions of layered materials by fitting the b parameter to obtain a good description of properties of these materials, after which the performance of the obtained functional is usually also tested on properties of other systems[98,99]. In the spirit of our SRP-DFT method, as described below we take an even more extreme approach to determining the b parameter.

The goal of the present paper is to investigate whether adding non-local rVV10 correlation to the MS mGGA functionals previously developed by us leads to functionals giving a better description of dissociative chemisorption of H_2 on the noble metal surfaces Cu(111), Ag(111), Au(111) and Pt(111). With this goal in mind, we investigated how closely we could reproduce the van der Waals interaction for the system for which the most accurate experimental results are available for this interaction (H_2 + Cu(111), van der Waals well depths and geometries are available from RMSA[80] or CMSA[91,92] experiments on this system). An additional reason for our choice of strategy is that most general

purpose DFs (at the GGA or mGGA level) cannot describe the interaction of H_2 with transition metal surfaces to within chemical accuracy (see for example figure 3.11 of Chapter 3 or figure 1a of Ref.[13]). Therefore closely reproducing reference data for gas phase dimers offers no guarantee that the obtained b value would be the best possible for H_2 + transition metal systems (although we will see below that this strategy would have worked for our case). However, we do check that the b parameter we adopt by considering the long range attractive van der Waals interaction also yields a reasonably good description of the metal lattice constant for copper, which is a short-to-medium range interaction, to make sure that "the tail does not wag the dog"[38].

Our tests on H_2 + Cu(111) were first done with the MS-PBEl-rVV10 DF (see figure 6.2). Adopting the b parameter of the original full rVV10 functional[48] ($b = 6.3$) yields a good description of the van der Waals well depth and minimum geometry, while a still reasonable lattice constant is obtained for copper (see figure 6.2 and below). However, optimizing the b parameter for the MS-B86bl-rVV10 and MS-RPBEl-rVV10 functionals in this manner poses a dilemma. Using the small values of b suggested by a requirement of closely reproducing the H_2 + Cu(111) van der Waals interaction leads to an underestimation of the copper lattice constant that we deem unacceptable (see figures 6.3-6.4). This dilemma is illustrated in figures 6.3-6.4, in which the lattice constant, the van der Waals well depth and the position of the van der Waals minimum are shown as a function of b for the MS-B86bl-rVV10 and the MS-RPBEl-rVV10 DFs. In these figures and figure 6.2 the lattice constant has been recalculated for each value of b, after which the 6 layer metal slabs are relaxed accordingly, and the van der Waals curve is calculated for a geometry in which H_2 is parallel to the surface and above the top site. From figures S1-3 it is clear that reducing b yields smaller lattice constants and deeper van der Waals wells that are closer to the surface. Keeping these observations in mind, and noting that fitting the b parameters for the MS-PBEl-rVV10 DF to either the van der Waals well depth or the position of the minimum would have resulted in a value that is very similar to the original value of Sabatini et al.[48] ($b = 6.3$), we simply chose to adopt this value for all three functionals.

Finally, we note that the original MS mGGA exchange-correlation functionals appear to meet the same criterion as the semi-local exchange-correlation functional used by Vydrov et al.[49] and Sabatini et al.[48], i.e. that this functional does not yield an attractive long range interaction (see figure 5.3b of Chapter 5). As Vydrov et al.[49] point out: 'it is preferable to combine VV10 with a functional that gives no significant binding in van der Waals complexes'. As our SLFs meet this criterion, we are not surprised that these SLFs combined with the NLC rVV10 functional yield either a good (with MS-PBEl) or still reasonable

(with MS-B86bl or MS-RPBEl) description of the van der Waals interaction in H_2 + Cu(111) with the choice of the original value of the b parameter.

6.2.3 Construction of the PESs

We use the corrugation reducing procedure (CRP)[109] to interpolate DFT results calculated on a grid in order to obtain a continuous representation of the PESs used in this work. Apart from using denser grids to improve the accuracy of the interpolated PESs our method is analogous to the one used by Wijzenbroek et al.[110]. In principle we use the grids reported in appendix 5.A of Chapter 5.

In Chapter 5 we have assessed the quality of the H_2 + Cu(111) PES obtained using the B86SRP68-DF2 DF by using ∼4900 randomly sampled geometries of H_2 above the metal slab. Based on all the randomly sampled points taken together our CRP[109] fit had a root mean square (rms) error of 31 meV compared to the underlying electronic structure calculations. When only looking at the 3538 geometries that have an interaction energy of H_2 with the surface lower then 4 eV the rms error reduces to 8 meV (∼ 0.2 kcal/mol). Since we use the same interpolation grids as in Chapter 5, we presume the accuracy of the obtained CRP PESs in this Chapter to be similar.

6.2.4 Quasi-classical dynamics

We compute observables using the quasi-classical trajectory (QCT) method[111]. This means that we take into account the quantum mechanical energies of the impinging H_2 and D_2 molecules in their initial rovibrational states. The method used is described more fully in section 2.3.1 of Chapter 2. We integrate the equations of motion using the algorithm of Stoer et al.[112].

In order to obtain reliable statistics we propagate 200,000 trajectories per energy point when simulating a molecular beam experiment, and 50,000 trajectories per energy point when calculating initial-state resolved reaction probabilities. Trajectories always start in the gas phase ($Z_{\text{gas}} = 8$Å). When r becomes bigger than some critical value ($r_c = 2.2$Å) the trajectory is counted as reacted. If during the propagation Z becomes bigger than Z_{gas} the trajectory is counted as scattered. In all QCT calculations we use a time step of $dt = 0.001$ fs. The reaction probability P_r is then calculated by dividing the number of reacted trajectories N_r by the total number of trajectories N_{total}

$$P_r = \frac{N_r}{N_{\text{total}}}. \tag{6.7}$$

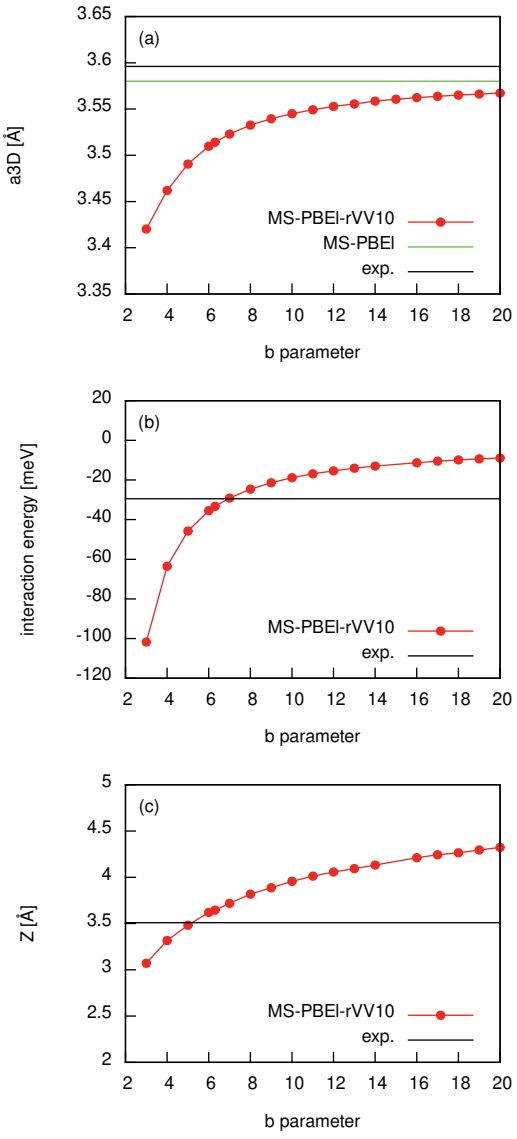

FIGURE 6.2: The lattice constant of copper in Å (a), and, for H_2 + Cu(111), the van der Waals well depth in meV (b) and the position of the van der Waals minimum in Å (c) are presented as calculated with the MS-PBEl-rVV10 DF. Calculated results are shown in red, experimental results are shown in black[89,108]. The green line in panel (a) shows the lattice constant obtained with the MS-PBEl DF[25].

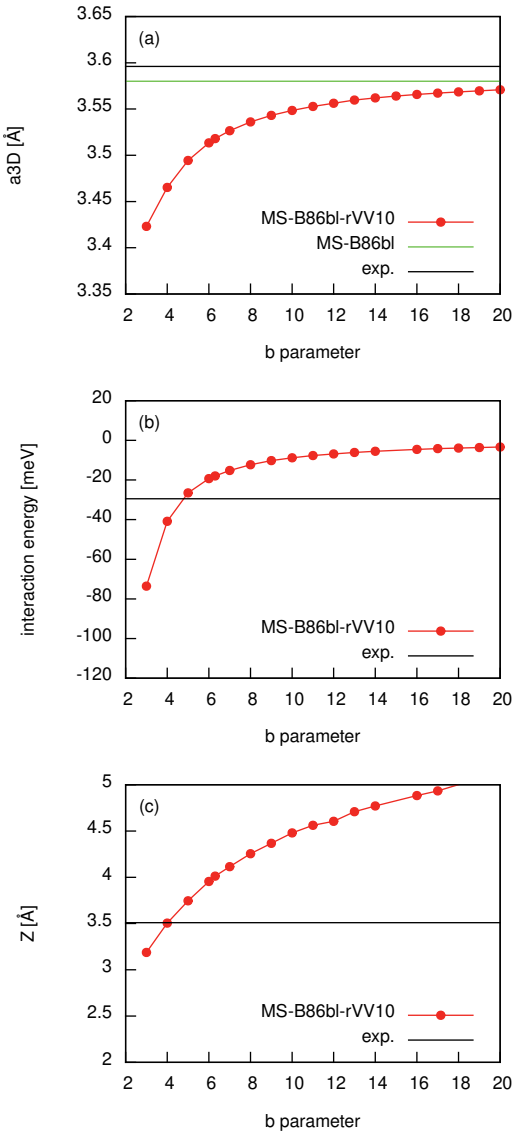

FIGURE 6.3: The lattice constant of copper in Å (a), and, for H_2 + Cu(111), the van der Waals well depth in meV (b) and the position of the van der Waals minimum in Å (c) are presented as calculated with the MS-B86bl-rVV10 DF. Calculated results are shown in red, experimental results are shown in black[89,108]. The green line in panel (a) shows the lattice constant obtained with the MS-B86bl DF[25].

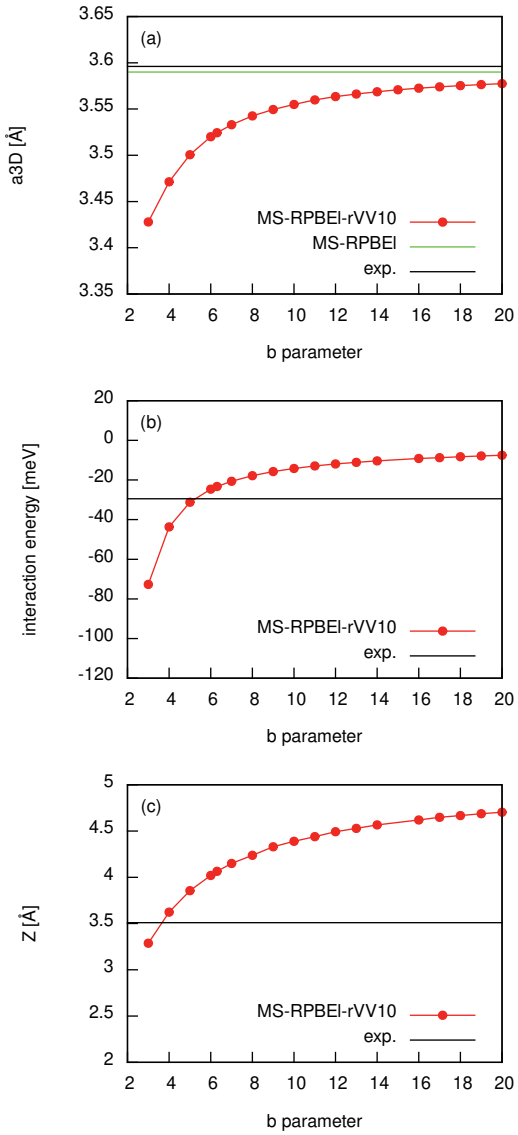

FIGURE 6.4: The lattice constant of copper in Å (a), and, for H_2 + Cu(111), the van der Waals well depth in meV (b) and the position of the van der Waals minimum in Å (c) are presented as calculated with the MS-RPBEl-rVV10 DF. Calculated results are shown in red, experimental results are shown in black[89,108]. The green line in panel (a) shows the lattice constant obtained with the MS-RPBEl DF[25].

6.2.5 Computation of observables

Molecular beam sticking

In the molecular beams we simulate, the probability to find H_2 with a velocity v in an interval $v + dv$ and in a particular rovibrational state at a given nozzle temperature T_N can be described by:

$$P(v_0, \alpha, \nu, J, T_n)dv = \underbrace{Cv^3 e^{-(v-v_0)^2/\alpha^2} dv}_{P_{flux}(v,\alpha)} \times P_{int}(\nu, J, T_n)dv \tag{6.8}$$

where C is a normalization constant, v_0 is the stream velocity and α is the width of the velocity distribution. With equation 6.8 the reactivity of each state can be weighted according to its Boltzmann weight as:

$$P_{int}(\nu, J, T_n) = \frac{g_N f(\nu, J, T_n)}{Z(T_n)} \tag{6.9}$$

with

$$f(\nu, J, T_n) = (2J+1) \times e^{(-(E_{\nu,0}-E_{0,0})/k_B T_{vib})} \times e^{(-(E_{\nu,J}-E_{\nu,0})/k_B T_{rot})}. \tag{6.10}$$

Here, the factor g_N in equation 6.9 reflects the ortho/para ratio of hydrogen in the beam. For D_2 $g_N = 2/3(1/3)$ for even (odd) values of J, while for H_2 $g_N = 1/4(3/4)$ for even (odd) values of J. $Z(T_n)$ is the partition function, k_B is the Boltzmann constant, and $E_{\nu,J}$ is the energy of the rovibrational state characterized by the vibrational (ν) and rotational (J) quantum numbers. In equation 6.10 we take into account the rotational cooling of the H_2 molecules due to the supersonic expansion by taking $T_{rot} = 0.8 * T_n$[31]. Degeneracy averaged reaction probabilities are computed from fully initial-state resolved reaction probabilities as:

$$P_{\text{deg}}(E, \nu, J) = \sum_{m_J=0}^{J} (2 - \delta_{m_J 0}) \frac{P_r(E, \nu, J, m_J)}{2J+1}, \tag{6.11}$$

where $P_r(E, \nu, J, m_J)$ is the fully initial-state resolved reaction probability, with m_J being the magnetic rotational quantum number and $E = \frac{1}{2}mv^2$ being the translational energy. Molecular beam sticking probabilities can then be computed as:

$$S_0(v_0, \alpha, T_N) = \sum_{\nu,J} \int P(v_0, \alpha, \nu, J, T_n) P_{\text{deg}}(E, \nu, J) dv. \tag{6.12}$$

All parameters describing the molecular beams simulated in this work are listed in table 5.4 of Chapter 5. A more exhaustive description of how molecular beam sticking probabilities can be computed can be found in Ref.[113] The set of initial rovibrational states taken into account in the QCT calculations is listed in table 5.3 of Chapter 5.

Rovibrational state populations of H_2 and D_2 desorbing from Au(111)

The following expression is used to calculate state distributions of desorbing molecules:[69]

$$N(\nu, J) = \int_0^{E_{\max(\nu,J)}} P_{int}(\nu, J, T_S)\sqrt{E}\, e^{(-\frac{E}{k_B T_S})}\, P_{\deg}(E, \nu, J) dE. \qquad (6.13)$$

Here $E_{\max}(\nu, J)$ is the maximum kinetic energy to which the experiment was sensitive[69] in the sense that $P_{\deg}(E, \nu, J)$ could still be extracted reliably, and these parameters have been obtained in a private communication[114]. T_S is the surface temperature. The $E_{\max}(\nu, J)$ parameters for H_2 (D_2) + Au(111) are plotted in figure 5.B.2 of Chapter 5. While Shuai et al.[69] integrated equation 6.13 up to 5 eV, we opt to integrate only until $E_{\max}(\nu, J)$ since the error function expressions derived in Ref.[69] are only reliable up to $E_{\max}(\nu, J)$ and can yield sticking probabilities substantially bigger than one for high translational energies. We integrate equation 6.13 by taking a right Riemann sum with a ΔE of 0.2 meV. The $N(\nu, J)$ populations are normalized to the total $\nu = 0$ population, as was done in Chapter 5. The ratios of populations we calculate are solely based on the rovibrational states shown in figure 6.12, i.e., we only go up to $J = 7$ for H_2 and $J = 9$ for D_2 as was done by Shuai et al.[69].

$E_{1/2}(\nu, J)$ **parameters**

In Chapter 5 we listed four possible methods to obtain $E_{1/2}(\nu, J)$ parameters which can be used to compare to experimental $E_0(\nu, J)$ parameters[15]. In this Chapter we only use method B2 to compare calculated $E_{1/2}(\nu, J)$ parameters to measured $E_0(\nu, J)$ parameters for the H_2 (D_2) + Au(111) system. All four methods are discussed in Chapter 5, and we will only briefly discuss method B2 here.

When no measured sticking probabilities are available for the system of interest one may choose to normalize the extracted reaction probabilities with reference to theory[69,72]. In method B1 theory is compared to experiment by

extracting $E_{1/2}(\nu, J)$ parameters using:

$$P_{deg}(E_{1/2}(\nu, J), \nu, J) = \frac{1}{2} A^{\mathrm{B1}}_{\nu,J} = \frac{1}{2} P_{deg}(E_{\max}(\nu, J), \nu, J). \tag{6.14}$$

In other words, the $E_{1/2}(\nu, J)$ parameter is the energy at which the degeneracy averaged reaction probability is equal to half the saturation value, which is taken equal to the reaction probability at the maximum kinetic energy to which the experiment was sensitive.

However, for H_2 (D_2) + Au(111) the $E_{\max}(\nu, J)$ parameters are not large enough to reliably extract $E_{1/2}(\nu, J)$ parameters[15]. In method B2 the measured $E_0(\nu, J)$ and $W_{\nu,J}$ values are therefore used to determine the $A^{\mathrm{B2}}_{\nu,J}$ value at which the experimental reaction probability saturates according to the error function fit of the (ν, J) rovibrational state[15,69]. Effectively, in method B2, we take the $A^{\mathrm{B1}}_{\nu,J}$ value and scale it accordingly[15]:

$$A^{\mathrm{B2}}_{\nu,J} = \frac{A^{\mathrm{B1}}_{\nu,J}}{\frac{1}{2} + \frac{1}{2} erf\left(\frac{E_{\max}(\nu,J) - E_0(\nu,J)}{W_{\nu,J}}\right)} \tag{6.15}$$

6.2.6 Computational details

A user modified version 5.4.4 of the Vienna Ab Initio Simulation Package[115–118] (VASP) has been used for all plane wave periodic DFT electronic structure calculations. The modification of the computer package concerns the implementation of the mGGA DFs developed in Chapter 3 and this Chapter. In all calculations the standard projector augmented wave (PAW) potentials[119] are used. We use the rVV10[48] non-local correlation functional as implemented in VASP[38], which is based on the vdW-DF1[94,120,121] implementation by Klimeš et al.[122]

All calculations are carried out using a plane wave cutoff energy of 600 eV together with smearing of 0.2 eV using the Methfessel-Paxton method of order one. All slabs consist of six layers, of which the bottom two layers are fixed at their ideal bulk interlayer distance. A 2×2 supercell is used for calculations of the PESs with a vacuum distance of 16 Å and a $(11 \times 11 \times 1)\Gamma$-centered k-point grid. Lattice constants have been calculated using four atom bulk unit cells and a $(28 \times 28 \times 28)$ Monckhorst-Pack k-point grid, while slab relaxations were carried out using a $(32 \times 32 \times 32)\Gamma$-centered k-point grid together with a 1×1 supercell. For the molecule-metal surface calculations a convergence parameter of 10^{-6} eV was used, and for the bulk lattice calculations, the slab relaxations

and the metal-atom calculations a convergence parameter of 10^{-7} eV was used for the energy.

6.3 Results and Discussion

6.3.1 Metal properties

Table 6.1 shows the calculated lattice constants compared to zero-point energy corrected experimental results[108] for the three MS mGGA-rVV10 DFs tested in this work as well as the original three MS mGGA DFs. For the four metals investigated here we calculate lattice constants that are smaller than the zero-point energy corrected experimental results, although the agreement with experiment[108] is still reasonable. The underestimation of the experimental lattice constants for the three DFs developed here is, on average, comparable to the somewhat overestimation of the lattice constants for SRP DFs designed for the reaction of H_2 (D_2) on transition metals at the GGA level that include non-local correlation[15] (see table 5.5 of Chapter 5).

Table 6.2 shows the interlayer contractions for the top two layers (in %) for Cu(111), Ag(111), Au(111) and Pt(111). When combining our three MS mGGA DFs[25] with rVV10[48] non-local correlation we find that the relaxed six layer slabs tend to expand somewhat, in contrast to the results obtained when not using non-local correlation[15,25]. The description of the relaxed slabs is not as good as obtained with previously developed SRP DFs[15], and with our mGGA DFs not using non-local correlation[25] (see table 6.2).

The three original MS mGGA DFs of Chapter 3 were developed to avoid having to compromise between a good description of the metal and a good description of the molecule-surface interaction[17]. It is therefore a somewhat disappointing result that when our three mGGA DFs are combined with non-local rVV10 correlation[48] this comes at the cost of a somewhat less good description of the metal. Tuning the b parameter in the implementation of rVV10 non-local correlation[48], which modulates the repulsive part of the van der Waals description[48], in order to obtain lattice constants closer to experiment unfortunately has the effect of removing the van der Waals wells in the PESs we calculate.

Including non-local correlation in a DF has a tendency to yield smaller lattice constants compared to DFs that do not include non-local correlation[15,108]. Our original MS mGGA DFs yield calculated lattice constants that are highly accurate[25]. Therefore combining them with non-local correlation, which tends to shrink the lattice constants, leads to too small calculated lattice constants.

	Cu		Ag		Au		Pt	
	Å	%	Å	%	Å	%	Å	%
exp.[108]	3.596		4.062		4.062		3.913	
MS-PBEl[25]	3.580	-0.4	4.090	0.7	4.084	0.5	3.906	-0.2
MS-PBEl-rVV10	3.514	-2.2	4.003	-1.4	4.034	-0.7	3.879	-0.9
MS-B86bl[25]	3.583	-0.4	4.092	0.7	4.087	0.6	3.908	-0.1
MS-B86bl-rVV10	3.518	-2.2	4.004	-1.4	4.036	-0.6	3.881	-0.8
MS-RPBEl[25]	3.590	-0.2	4.099	0.9	4.092	0.7	3.912	0
MS-RPBEl-rVV10	3.524	-2.0	4.008	-1.3	4.040	-0.5	3.884	-0.7

TABLE 6.1: Calculated lattice constants in Å compared to to zero-point energy corrected experimental results[108]. Percentage deviations of the computed results from experimental results are also indicated.

We also observe that the interlayer distance between the top two layers of the relaxed six layer slabs tend to expand somewhat when using rVV10[48] non-local correlation (see table 6.2). When not using non-local correlation our three MS mGGA DFs produced interlayer distances between the top layers that were in line with experimental results[15,25]. When using rVV10[48] non-local correlation together with our MS mGGA DFs our calculated interlayer distances of the top layer are still reasonable, although not as good as those obtained with GGA based SRP DFs that use vdW-DF1[94] or vdW-DF2[95] non-local correlation (see table 5.6 of Chapter 5). We speculate that the more accurate interlayer distances calculated when using vdW-DF1[94] or vdW-DF2[95] non-local correlation are due to the way in which the correlation part of the full exchange correlation functional is constructed. In the case of vdW-DF1[94] or vdW-DF2[95] the non-local correlation part is combined only with fully local LDA correlation. In the case of the MS mGGA-rVV10 functionals that we test here, the NLC rVV10 functional is combined with semi-local correlation instead (see Eq. 6.4 above). For calculating lattice constants and interlayer spacings of metals it might be better to combine the MS meta-GGA exchange functionals we investigate with correlation functionals based on LDA correlation and a non-local van der Waals correlation functional.

6.3.2 Static PES properties

Figure 6.5 shows van der Waals wells for H_2 in a parallel ($\phi = 0°, \theta = 90°$) and in the perpendicular ($\theta = 0°$) orientation above a top site for Cu(111) (a), Ag(111) (b), Au(111) (c) and Pt(111) (d). All van der Waals well geometries and well depths computed by us are tabulated in table 6.3, also comparing with experimental results that have been reported for H_2 + Cu(111)[89,90], H_2 + Ag(111)[84], H_2 + Au(111)[90] and H_2 + Pt(111)[81,93]. Note that we use the same b value ($b = 6.3$) for the three DFs that use rVV10[48] non-local correlation.

	Cu	Ag	Au	Pt
exp.	-1.0%,[123,124] -0.7%[125]	-2.5%,[126] -0.5%[127]	1.5%[128]	1.1%[129]
MS-PBEl[25]	-1.0%	-0.4%	1.0%	1.0%
MS-PBEl-rVV10	1.5%	2.3%	3.5%	2.4%
MS-B86bl[25]	-1.0%	-0.5%	1.0%	1.0%
MS-B86bl-rVV10	1.4%	1.4%	3.5%	2.3%
MS-RPBEl[25]	-1.6%	-0.5%	1.2%	1.1%
MS-RPBEl-rVV10	1.6%	2.4%	3.5%	2.4%

TABLE 6.2: Relaxations of the interlayer distance of the top two layers relative to the the bulk interlayer distance in %. Computed results are shown for six DFs and compared with experimental values.

As noted in Chapter 5, for Cu(111) the experimental well depths are in good agreement. However, the position reported by Harten et al.[90] is somewhat closer to the surface. Ambiguities in the level assignments in the study of Andersson et al.[88] is the mostly likely reason for the van der Waals well being reported somewhat closer to the surface compared to the later measurements[89]. Andersson et al.[89] noted that their derived PES is also consistent with the earlier measurements[88]. As mentioned in Chapter 5, we suspect that reported van der Waals wells for H_2 + Ag(111)[84] and H_2 + Au(111)[90] might possibly be too close to the surface[88].

The MS-PBEl-rVV10 DF performs best with respect to the van der Waals well interaction for all systems investigated. Highly accurate van der Waals well depths are obtained for both the highly activated systems and the non-activated H_2 + Pt(111) system with this functional (see figure 6.5 and table 6.3). The agreement with the position of the minimum is also good for the system for which this is well-known, i.e., H_2 + Cu(111). The agreement with the experimental well depth obtained with the MS-B86bl-rVV10 and MS-RPBEl-rVV10 DFs is reasonable. This agreement is not as good as obtained with the MS-PBEl-rVV10 DF, but the MS-RPBEl-rVV10 results agree better with the experimental results for the well depths for H_2 + Ag(111) and Au(111) than the results previously obtained with the vdW-DF1 functional (see table 6.3 and figures 6.5b and 6.5c). As discussed above, optimization of the b parameter to better reproduce the well depth obtained with the MS-B86bl-rVV10 and MS-RPBEl-rVV10 DFs would result in unacceptably small lattice constants.

When comparing the results it is clear that the MS-PBEl-rVV10 DF yields a better description of the H_2-metal van der Waals wells investigated here than the vdW-DF1[94] and vdW-DF2[95] DFs, which is consistent with earlier work[48] on the binding energies of a subset of molecular configurations of the S22 data set[105] and the argon dimer[48]. However, we note that the previously

tested[15] B86SRP68-DF2 DF (which performed best of the vdW-DF1[94] and vdW-DF2[95] DFs tested in 5) shows a performance that is comparable to that of the MS-PBEl-rVV10 DF (table 6.3). We also note that the polarizability obtained for the H_2 molecule parallel and perpendicular to its molecular axis is similar for the MS-PBEl-rVV10 and vdW-DF2[95] DFs.

In principle the b parameter in the rVV10[48] non-local correlation functional could be tuned to match experimental observations of the van der Waals geometries in future work. However, decreasing the b parameter to obtain a van der Waals well geometry more in line with experiment would also lead to further decreased lattice constants thereby further worsening the agreement with experiment, and it would lead to lower dissociation barriers.

Tables 6.4-6.7 show barrier heights and geometries for H_2 + Cu(111), Ag(111), Au(111) and Pt(111), respectively. For the activated systems the lateness of the barriers (values of r at which the barriers occur) is not influenced by the use of rVV10[48] non-local correlation. However, for the bridge sites the barrier geometries do move to slightly higher Z values. Adding rVV10[48] non-local correlation to our original three MS mGGA DFs yields barrier heights that are consistently lower by roughly 0.15-0.2 eV for the highly activated systems. For the barrier heights obtained with the current best SRP-DFs we refer the reader to Chapter 5.

For the non-activated H_2 + Pt(111) system we also find that using rVV10[48] non-local correlation leads to lower barriers, by about 0.15 eV. However the picture is more complex since only three DFs show a double barrier structure for the t2b site, namely the MS-PBEl[25], MS-B86bl[25] and MS-PBEl-rVV10 DFs. The DFs without non-local correlation do not show a double barrier structure for the t2h site, while the DFs that do use rVV10[48] non-local correlation do.

Note that observations on the van der Waals well depths and minimum positions extracted from RMSA[80] or CMSA[91,92] experiments usually represent averages taken over the sites in the surface unit cell. Checking for the site-dependence of the van der Waals interaction in H_2 + Cu(111), as found by Lee et al.[130], we see essentially no dependence of the van der Waals interaction on the site within the unit cell (see figure 6.6, which presents results for impact on three different sites obtained with the MS-PBEl-rVV10 DF). The site dependence found for the other systems and DFs treated here is similar to the results shown in figure 6.6 in that it is very small.

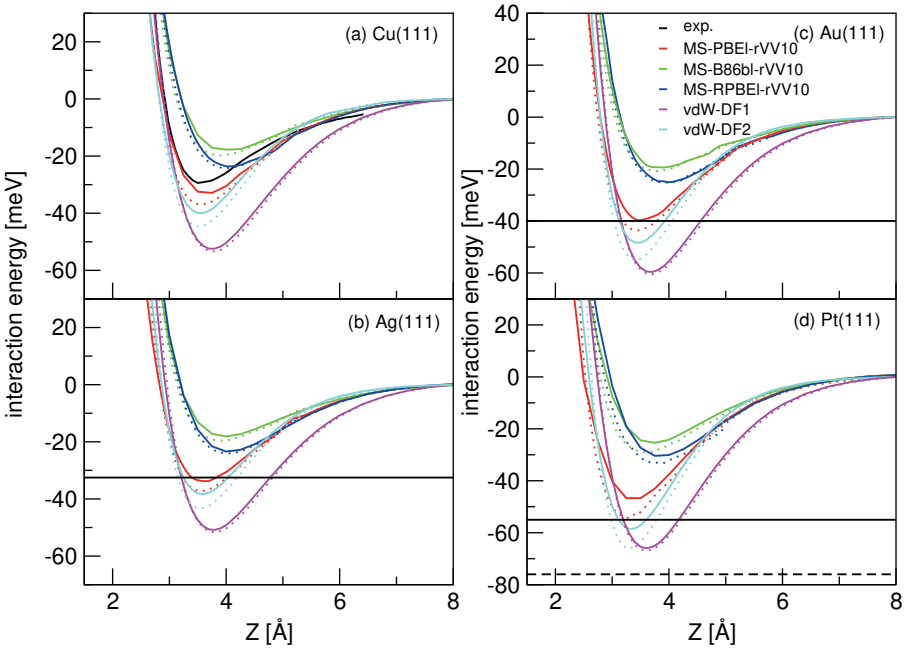

FIGURE 6.5: Van der Waals potential curves for H_2 + Cu(111) (a), Ag(111) (b), Au(111) (c) and Pt(111) (d). Solid lines represent a parallel orientation of H_2 ($\theta = 90°$, $\phi = 0°$) and dotted lines a perpendicular orientation ($\theta = 0°$), both above a top site. Experimental results are shown in black for H_2 + Cu(111)[89], H_2 + Ag(111)[84], H_2 + Au(111)[90] and H_2 + Pt(111)[81,93]. In panels b and c the horizontal solid lines correspond to the experimental well depths. In panel d the dashed line corresponds to the result of Poelsema et al.[93] and the solid line corresponds to the result of Cowin et al.[81]. Results for five DFs are shown: MS-PBEl-rVV10 (red), MS-B86bl-rVV10 (green), MS-RPBEl-rVV10 (blue), vdW-DF1[94] (magenta) and vdW-DF2[95] (light blue).

Cu(111)	Z [Å]	E_{vdW} [meV]
exp.	3.51[89], 2.71[90]	29.5[89], 22.2[90]
MS-PBEl-rVV10	3.66	33.1
MS-B86bl-rVV10	3.99	18.2
MS-RPBEl-rVV10	4.05	23.7
vdW-DF1[94]	3.77	52.4
vdW-DF2[95]	3.58	39.0
Ag(111)		
exp.[84]	1.98	32.5
MS-PBEl-rVV10	3.66	33.8
MS-B86bl-rVV10	4.02	18.4
MS-RPBEl-rVV10	4.04	23.4
vdW-DF1[94]	3.77	50.8
vdW-DF2[95]	3.58	38.3
Au(111)		
exp.[90]	2.2	40.0
MS-PBEl-rVV10	3.48	39.7
MS-B86bl-rVV10	3.90	19.4
MS-RPBEl-rVV10	4.04	25.2
vdW-DF1[94]	3.68	59.7
vdW-DF2[95]	3.45	48.5
Pt(111)		
exp.		55[81], 76[93]
MS-PBEl-rVV10	3.35	50.5
MS-B86bl-rVV10	3.30	26.9
MS-RPBEl-rVV10	3.88	32.3
vdW-DF1[94]	3.61	65.9
vdW-DF2[95]	3.36	58.6

TABLE 6.3: Van der Waals well depths and positions for Cu(111), Ag(111), Au(111) and Pt(111) for H_2 in parallel orientation ($\phi = 0°, \theta = 90°$) above a top site.

	bridge			t2b			fcc		
	E_b	r_b	Z_b	E_b	r_b	Z_b	E_b	r_b	Z_b
MS-PBEl[25]	0.629	1.002	1.198	0.847	1.350	1.390	0.988	1.339	1.267
MS-PBEl-rVV10	0.459	0.985	1.240	0.665	1.328	1.400	0.815	1.331	1.285
MS-B86bl[25]	0.683	0.997	1.205	0.895	1.351	1.391	1.048	1.343	1.267
MS-B86bl-rVV10	0.513	0.982	1.247	0.714	1.329	1.401	0.865	1.333	1.285
MS-RPBEl[25]	0.721	1.006	1.201	0.930	1.354	1.392	1.086	1.346	1.270
MS-RPBEl-rVV10	0.549	0.985	1.247	0.747	1.329	1.403	0.899	1.334	1.286

TABLE 6.4: Barrier height for H_2 reacting on Cu(111), for the bridge, t2b and fcc sites $\phi = 0°$ and $\theta = 90°$. Barrier heights are in eV, and the barrier positions in Å.

	bridge			t2b			fcc		
	E_b	r_b	Z_b	E_b	r_b	Z_b	E_b	r_b	Z_b
MS-PBEl[25]	1.288	1.230	1.116	1.534	1.508	1.493	1.601	1.556	1.315
MS-PBEl-rVV10	1.082	1.224	1.157	1.328	1.486	1.506	1.392	1.553	1.345
MS-B86bl[25]	1.342	1.224	1.115	1.585	1.513	1.495	1.652	1.566	1.323
MS-B86bl-rVV10	1.134	1.223	1.159	1.376	1.488	1.507	1.442	1.560	1.348
MS-RPBEl-rVV10	1.171	1.226	1.161	1.410	1.489	1.508	1.479	1.560	1.349

TABLE 6.5: Barrier height for H_2 reacting on Ag(111), for the bridge, t2b and fcc sites $\phi = 0°$ and $\theta = 90°$. Barrier heights are in eV, and the barrier positions in Å.

	bridge			t2b			fcc		
	E_b	r_b	Z_b	E_b	r_b	Z_b	E_b	r_b	Z_b
MS-PBEl[25]	1.432	1.144	1.127	1.301	1.433	1.466	1.350	1.203	1.276
MS-PBEl-rVV10	1.251	1.148	1.159	1.139	1.425	1.475	1.172	1.216	1.299
MS-B86bl[25]	1.481	1.142	1.130	1.355	1.438	1.467	1.402	1.204	1.276
MS-B86bl-rVV10	1.302	1.147	1.162	1.192	1.427	1.476	1.224	1.216	1.299
MS-RPBEl-rVV10	1.336	1.147	1.163	1.226	1.436	1.476	1.258	1.219	1.302

TABLE 6.6: Barrier height for H_2 reacting on Au(111), for the bridge, t2b and fcc sites $\phi = 0°$ and $\theta = 90°$. Barrier heights are in eV, and the barrier positions in Å.

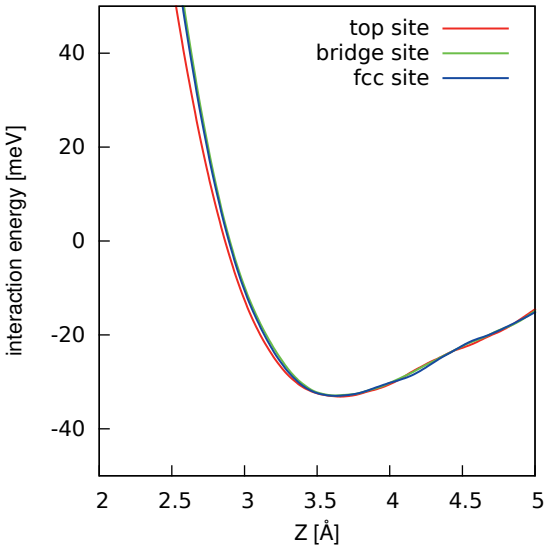

FIGURE 6.6: Van der Waals potential curves for H_2 ($\theta = 90°$, $\phi = 0°$) above Cu(111) for impact on the top, bridge and fcc sites for the MS-PBEl-rVV10 density functional.

	t2b early			t2b late			bridge			t2h early			t2h late		
	E_b	r_b	Z_b	E_b	r_b	Z_b	E_b	r_b	Z_b	E_b	r_b	Z_b	E_b	r_b	Z_b
MS-PBEl[25]	0.145	0.766	2.205	-0.035	1.096	1.529	0.616	0.838	1.599	0.339	0.800	1.840			
MS-PBEl-rVV10	0.008	0.763	2.326	-0.211	1.087	1.538	0.445	0.837	1.634	0.180	0.828	1.809	0.217	1.195	1.525
MS-B86bl[25]	0.194	0.768	2.189	0.016	1.085	1.534	0.667	0.839	1.602	0.392	0.802	1.836			
MS-B86bl-rVV10	0.056	0.763	2.313				0.493	0.836	1.633	0.235	0.820	1.846	0.263	1.205	1.525
MS-RPBEl-rVV10	0.071	0.769	2.230				0.521	0.841	1.624	0.261	0.830	1.805	0.319	1.211	1.526

TABLE 6.7: Barrier heights for H_2 reacting on Pt(111), for the bridge and t2b sites $\phi = 0°$ and $\theta = 90°$, and for the t2h site $\phi = 120°$. Barrier heights are in eV, and the barrier positions in Å. For the t2b and t2h geometry data is presented for the early and the late geometry when relevant.

6.3.3 Molecular beam sticking

Molecular beam sticking of H_2 (D_2) + Cu(111)

Molecular beam sticking probabilities for H_2 (D_2) + Cu(111) for six sets of molecular beam experiments are shown in figure 6.7 for the three MS mGGA-rVV10 DFs tested in this work and for the MS-B86bl and PBE DFs[25]. The parameters describing the molecular beam experiments[29–31] are tabulated in table 5.4 of Chapter 5. Adding rVV10[48] non-local correlation to our three original mGGA DFs leads to higher sticking probabilities that are too high compared to experiment, as could be expected from its effect on the barrier heights (see table 6.4). MS-PBEl-rVV10, MS-B86bl-rVV10 and MS-RPBEl-rVV10 all overestimate the sticking probability and are not chemically accurate for this system. Given that the original three MS mGGA DFs were all chemically accurate for this system[25] this is a somewhat disappointing result.

Molecular beam sticking of D_2 + Ag(111)

Figure 6.8 shows sticking probabilities computed from simulations of molecular beams of D_2 reacting on Ag(111) in comparison with experimental results[32]. Cottrell et al.[32] have reported molecular beam parameters that are symmetric with respect to the average collision energy. We consider these symmetric molecular beam parameters to be somewhat unphysical, as discussed in previous work from our group[64]. Therefore we opted to use the molecular beam parameters of pure D_2 reacting on Cu(111) reported by Auerbach and coworkers[29] (see table 5.4), which likewise describe beams that are narrow in translational energy, in our simulations.

MAD values are computed by calculating the mean distance along the incidence energy axis from the calculated sticking probability to the cubic spline interpolated experimental results. We consider DFs that yield a MAD value smaller than 1 kcal/mol (4.2 kJ/mol) to be chemically accurate[131]. Figure 6.8 shows that all three DFs can be considered chemically accurate for this system, with the MS-PBEl-rVV10 DF performing best with a MAD of 1.0 kJ/mol and the MS-RPBE-rVV10 DF performing worst with a still good MAD value of 2.0 kJ/mol. Here we note that the distance between the computed and the measured S_0 tends to increase with increasing translational energy.

This is the first time that we achieve a chemically accurate description of the D_2 + Ag(111) system. GGA based DFs with and without non-local correlation as well as the three original MS mGGA DFs have not been able to yield a chemically accurate description of this system[15,25,64]. The improved description of the sticking probability for this system is strictly due to the lowering of the

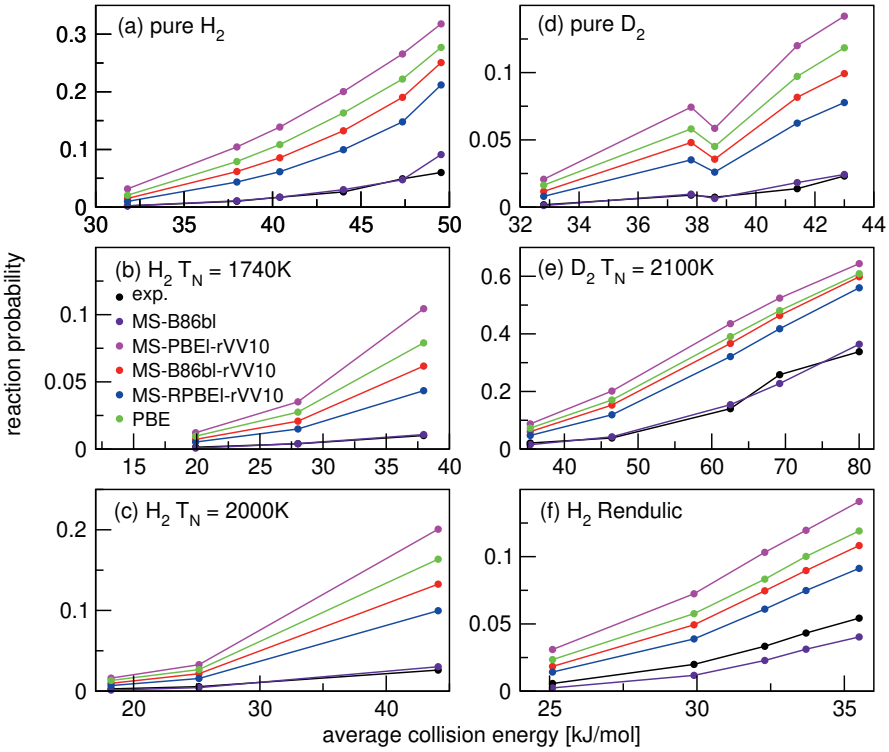

FIGURE 6.7: Molecular beam sticking probabilities for H_2 and D_2 reacting on Cu(111) for six sets of molecular beam experiments, as computed using the QCT method with the MS-B86bl[25] (purple), MS-PBEl-rVV10 (magenta), MS-B86bl-rVV10 (red), MS-RPBEl-rVV10 (blue) and PBE (green) DFs. Experimental results are shown in black[29–31].

barrier to reaction. Barrier geometries of the MS mGGA DFs that use non-local rVV10[48] correlation are very similar to the barrier geometries of the original MS mGGA DFs (see table 6.5).

As we discussed in previous work from our group[15,64] and Chapter 5, assessing the the quality of the theoretical description of this system is difficult due to the lack of well defined molecular beam parameters[64]. Additional experiments would allow us to improve the description of this system[15].

Molecular beam sticking of D_2 + Pt(111)

Figure 6.9 shows calculations on D_2 + Pt(111) for two sets of molecular beam experiments[66,67]. Note that this is a non-activated system of which the original MS mGGA DFs gave a rather poor description[15] (see Chapter 5). Here we find that the MS-B86bl-rVV10 DF (figures 6.9b,e) yields the best results for both experiments, with a MAD of 2.7 kJ/mol for the experiment of Luntz et al.[66] and a MAD of 2.0 kJ/mol for the experiments of Cao et al.[67]. This may be compared to the MAD values of 1.1 kJ/mol for the experiment of Luntz et al.[66] and of 1.9 kJ/mol for the experiment of Cao et al.[67] that were obtained with the PBEα57-DF2 DF[14].

In general the three MS mGGA-rVV10 DFs treated here are either in good agreement with experiment for the lower translational energies (MS-PBEl-rVV10) or for the higher translational energies (MS-B86bl-rVV10 and MS-RPBE-rVV10). The reason for this is that the MS-PBEl-rVV10 DF is the DF yielding the lowest early t2b barrier to reaction (see table 6.7), which allows it to describe the experiment correctly at the lowest translational energies. The other two mGGA-rVV10 DFs exhibit a higher early t2b barrier, leading to a worse description of the experiments[66,67] at low translational energies. Overal the slope of the calculated sticking probability curve of the MS-PBEl-rVV10 DF is too steep, just right for the MS-B86bl-rVV10 DF, and somewhat too gentle for the MS-RPBEl-rVV10 DF.

Previous work from our group has indicated that the experiments of Luntz et al.[66] and Cao et al.[67] are in good agreement with each other for the lower incidence energies but somewhat diverge for the higher incidence energies[132]. The possible causes for this divergence are discussed in Ref.[132], where it was remarked that at high incidence energies the reaction probabilities of Cao et al.[67] are most likely somewhat underestimated compared to the results of Luntz et al.[66]. Note that a small increase of reactivity at the higher translational energies for the experiments of Cao et al.[67] could improve the agreement with experiment for the MS-B86bl-rVV10 DF. However, this system is still best

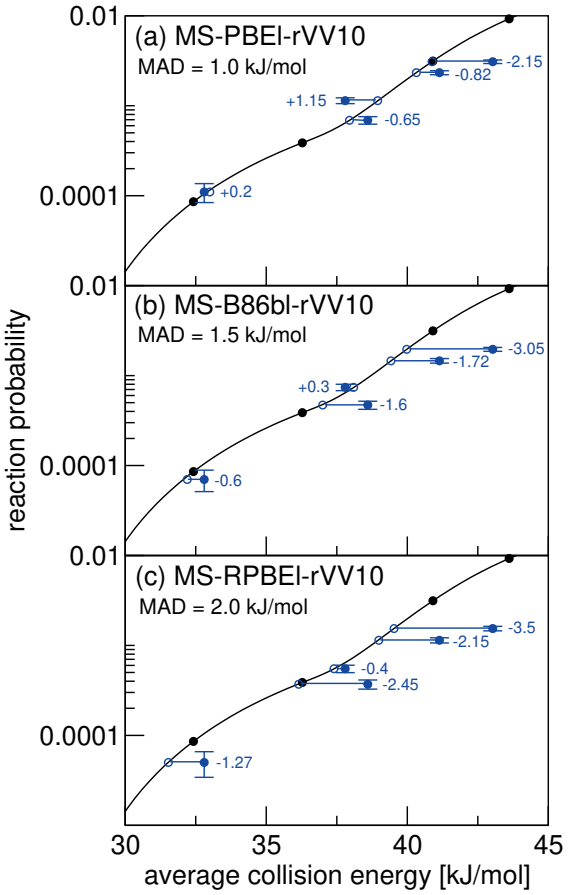

FIGURE 6.8: Molecular beam sticking probability as a function of the average incidence energy for D_2 reacting on Ag(111). Experiment is shown in black[32]. QCT results are shown in blue for the following DFs: MS-PBEl-rVV10 (a), MS-B86bl-rVV10 (b) and MS-RPBEl-rVV10 (c). The values next to each data point denote the shift along the translational energy axis from the computed reaction probability to the interpolated experimental reaction probability curve in kJ/mol.

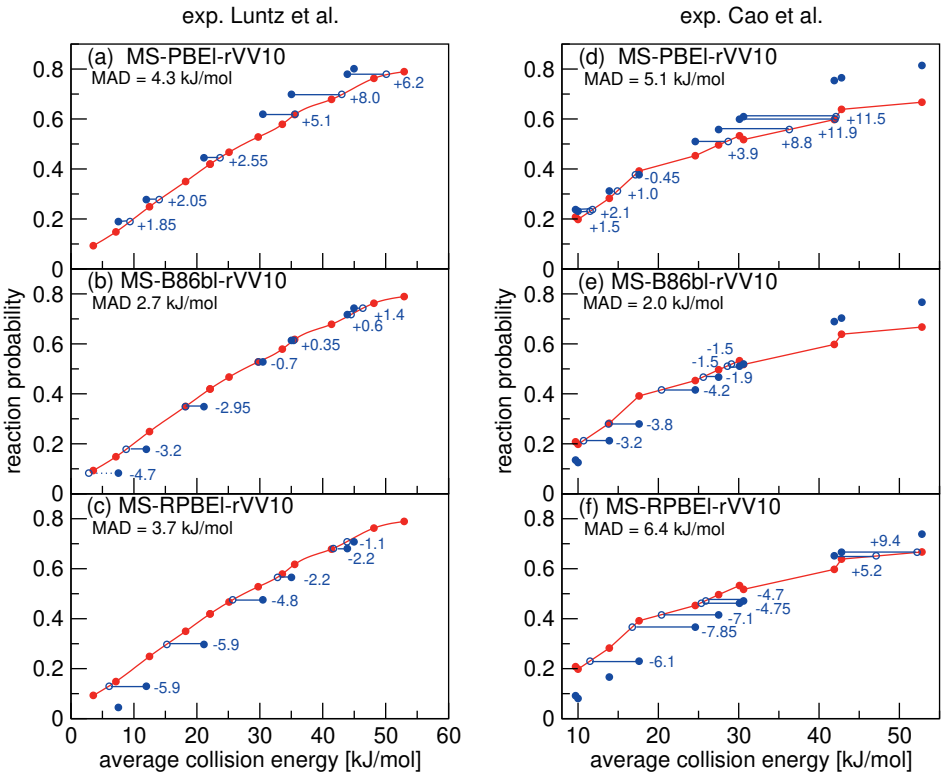

FIGURE 6.9: Molecular beam sticking probabilities for D_2 reacting on Pt(111) for the MS-PBEl-rVV10 (a,d), MS-B86bl-rVV10 (b,e) and MS-RPBEl-rVV10 (c,f) DFs. Experimental results are shown in red[66,67], QCT results in blue. The values next to each data point denote the shift along the translational energy axis from the computed reaction probability to the interpolated experimental reaction probability, curves in kJ/mol.

described with the GGA based SRP DF that was specifically designed for this system[14,132].

6.3.4 Associative desorption

3.4.1 Initial-state resolved reaction probabilities Ag(111)

Figure 6.10 shows degeneracy averaged initial-state resolved reaction probabilities for H_2 and D_2 reacting on Ag(111). A comparison is made to reaction probabilities extracted from associative desorption experiments assuming detailed balance[70,71]. Note that the experimental degeneracy averaged reaction

probabilities were not normalized but simply assumed to saturate at one, which makes it hard to make a comparison with experiment. The translational energy in figure 6.10 refers to the translational energy of the desorbing molecules which is measured by time-of-flight techniques[70,71].

From figure 6.10 it can be seen that the three MS mGGA-rVV10 DFs somewhat overestimate the degeneracy averaged reaction probabilities for D_2 for most energies (figure 6.10a,b), but that the agreement with experiment is very good for H_2 (figure 6.10c). In previous work[25] the MS-PBEl DF was shown to perform better than other GGA based DFs mainly due to MS-PBEl exhibiting slightly earlier barriers. The barrier geometries of the three MS mGGA-rVV10 DFs we present here are very similar to the barrier geometries of the three original MS mGGA DFs[25]. Therefore we can say safely that the increased reactivity obtained with the mGGA-rVV10 DFs developed here is due to their barriers to reaction being somewhat lower and not to a change in barrier geometry (see table 6.5).

$E_{1/2}(\nu, J)$ parameters Au(111)

Figure 6.11 shows a comparison of measured[69] $E_0(\nu, J)$ parameters to $E_{1/2}(\nu, J)$ parameters calculated using method B2[15]. Table 6.8 shows the accompanying MAD and mean signed deviations (MSD) values. We note that the experiment was performed at a surface temperature of 1063 K[69], while the calculations have been performed using the BOSS model. Furthermore, incorporating surface motion in the dynamics calculations would lead to a broadening of the reaction probability curves[22,51,52,55]. In view of the procedure used to calculate $E_{1/2}(\nu, J)$ parameters, an increase of reactivity at low translational energies has the potential to lower the $E_{1/2}(\nu, J)$ parameters[15]. We also note that our calculations have been carried out employing an unreconstructed Au(111) surface. Mapping out a full PES of H_2 interacting with reconstructed Au(111) is currently extremely hard to do if not impossible, due to the large unit cell size[15]. Earlier work in our group[133] has shown that dynamical barrier heights of reconstructed Au(111) are roughly 50 meV higher compared to unreconstructed Au(111), which would lead to slightly higher computed $E_{1/2}(\nu, J)$ parameters[15].

Even though all three developed MS mGGA DFs overestimate the measured $E_0(\nu, J)$ parameters, it is clear from table 6.8 that MS-PBEl-rVV10 achieves chemical accuracy here for H_2, and is just 1 meV shy of chemical accuracy (43 meV) for D_2. The MAD values of all three newly developed DFs are similar to the MAD values of PBE (46 meV for H_2 and 58 meV for D_2)[15]. Previously we have found that the original mGGA DFs as well as various GGA based SRP DFs that include non-local correlation overestimate the experimental $E_0(\nu, J)$

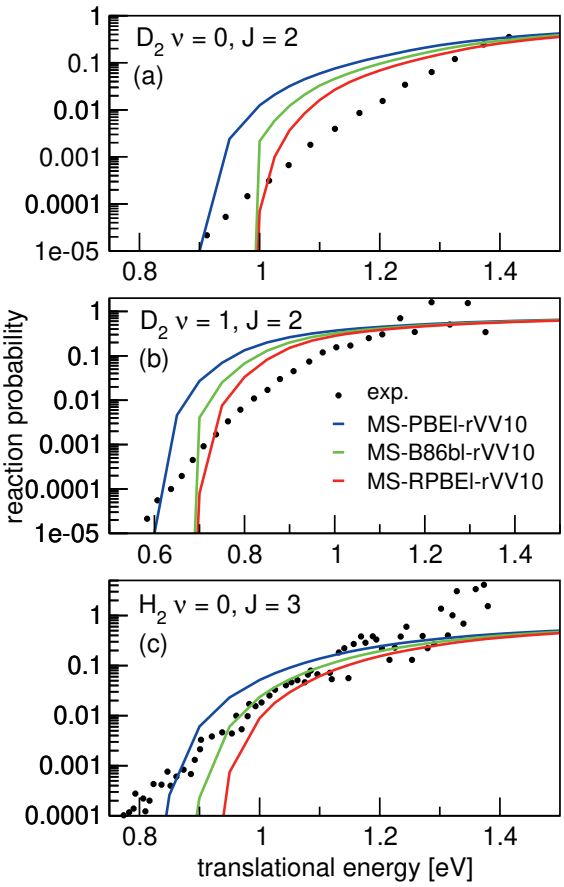

FIGURE 6.10: Initial-state selected reaction probabilities $P_{deg}(E, \nu, J)$ computed for H_2 (D_2) + Ag(111) using the MS-PBEl-rVV10 (blue), MS-B86bl-rVV10 (green) and MS-RPBEl-rVV10 (red) DFs as a function of translational energy are shown, comparing with values extracted from associative desorption experiments[70,71]. Results are shown for D_2 ($\nu = 0, J = 2$) (a), D_2 ($\nu = 1, J = 2$) (b), and H_2 ($\nu = 0, J = 3$) (c).

parameters by roughly 0.1 eV[15] (see figure 5.17 of Chapter 5). Furthermore, all three developed mGGA DFs reproduce the J dependence of the $E_0(\nu, J)$ parameters quite well. As discussed in Chapter 5, this suggests that the reactivities of the individual rovibrational states are well described relative to one another, as long as states are considered within the same vibrational level. Given the uncertainties involved in using method B2 to calculate $E_{1/2}(\nu, J)$ parameters, we obtain excellent results using our three newly developed MS mGGA-rVV10 DFs.

Previously reported experiments implied that the recombination of H_2 on Au(111) is coupled to the electronic degrees of freedom of the metal[134–137]. Currently we cannot disentangle the effects of ehp excitation, surface motion and surface reconstruction. In Chapter 5 we discussed how a combined analysis of a molecular beam dissociative chemisorption experiment on a reasonably cold surface (if available) and calculations on a reconstructed Au(111) surface, together with the associative desorption experiment of Shuai et al.[69] could in principle be used to obtain a fingerprint of ehp excitation. Additionally, if a molecular beam dissociative chemisorption experiment were to become available, this would allow us to assess if the absolute reactivity computed with the new mGGA-rVV10 DFs and shown here is accurate[15].

Rovibrational state populations of H_2 and D_2 desorbing from Au(111)

Rovibrational state populations for H_2 and D_2 desorbing from Au(111) are shown in figure 6.12. Here we plot $ln[N/g_N(2J+1)]$ versus the rotational energy, with N being the total population for each (ν, J) state and $g_N(2J+1)$ being the statistical weight for rotational level J[69]. In such a plot a Boltzmann distribution will appear as a straight line[69]. Shuai et al.[69] have used an upper integration limit of 5 eV. Since the error function fits of the experiment are only reliable below $E_{\max}(\nu, J)$, we opt to use $E_{\max}(\nu, J)$ as the upper integration limit, as we did in Chapter 5. Note that we use the same normalization procedure as in Chapter 5. The solid line represents a Boltzman distribution at the surface temperature of 1063 K used in the experiment[69].

For molecules in the vibrational ground state it can be seen that the rotationally excited molecules lie above the line set by the Boltzmann distributions. The experimental results lie on a gentler slope then the Boltzmann distributions, indicating that rotationally excited molecules are more likely to adsorb[69]. Similarly, the results for vibrationally excited molecules lie on a line with a gentler slope than shown by the Boltzmann distributions. Additionally the results for vibrationally excited molecules lie substantially above the line of Boltzmann

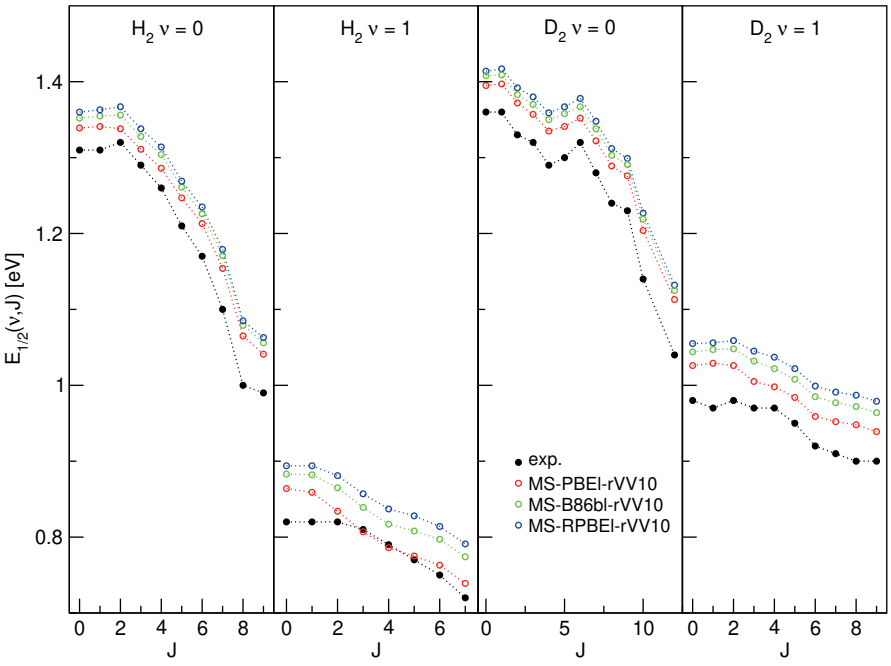

FIGURE 6.11: $E_{1/2}(\nu, J)$ parameters as a function of J obtained using method B2 for H_2 and D_2 reacting on Au(111). Experimental values are shown in black[69]. Red circles represent the MS-PBEl-rVV10 values, green circles the MS-B86bl-rVV10 values and blue circles the MS-RPBEl-rVV10 values.

Au(111)	MAD (eV) H_2			MSD (eV) H_2			MAD (eV) D_2			MSD (eV) D_2		
	total	$\nu = 0$	$\nu = 1$	total	$\nu = 0$	$\nu = 1$	total	$\nu = 0$	$\nu = 1$	total	$\nu = 0$	$\nu = 1$
MS-PBEl[25]	0.106	0.104	0.107	-0.106	-0.104	-0.107	0.092	0.084	0.100	-0.084	-0.056	-0.112
MS-PBEl-rVV10	0.029	0.038	0.018	-0.028	-0.038	-0.016	0.044	0.045	0.042	-0.044	-0.045	-0.042
MS-B86bl[25]	0.139	0.131	0.150	-0.139	-0.131	-0.150	0.112	0.100	0.127	-0.112	-0.100	-0.128
MS-B86b-rVV10	0.050	0.053	0.046	-0.050	-0.053	-0.046	0.061	0.059	0.065	-0.061	-0.059	-0.065
MS-RPBE-rVV10	0.062	0.061	0.062	-0.062	-0.061	-0.062	0.073	0.068	0.078	-0.073	-0.068	-0.078

TABLE 6.8: Mean absolute and mean signed deviations for the theoretical $E_{1/2}(\nu, J)$ parameters compared to experimental $E_0(\nu, J)$ values for Au(111)[69].

	H_2	D_2
exp.[69]	0.552	0.424
MS-PBEl[25]	0.178	0.387
MS-PBEl-rVV10	0.175	0.377
MS-B86bl[25]	0.176	0.379
MS-B86bl-rVV10	0.193	0.365
MS-RPBEl-rVV10	0.180	0.366

TABLE 6.9: The ratio of $\nu = 1 : \nu = 0$ molecules desorbing from Au(111) as measured in experiments[69] and computed with the MS-PBEl[25], MS-PBEl-rVV10, MS-B86bl[25], MS-B86bl-rVV10 and MS-RPBEl-rVV10 DFs.

distributions, thereby indicating that vibrationally excited molecules are more likely to adsorb[69].

Table 6.9 shows the $\nu = 1 : \nu = 0$ ratio of desorbing molecules, these ratios are calculated using the same rovibrational states as shown in figure 6.12. Note that the difference between the experimental values shown in table 6.9 and those reported by Shuai et al.[69] is due to using $E_{\max}(\nu, J)$ as the upper integration limit.

From figure 6.12 it is clear that the differences between all DFs shown is minimal, and that the agreement between theory and experiment is best for D_2. As was already reported by Shuai et al.[69], the theoretical ratios computed with different DFs for H_2 are much lower than the experimental ratio. In Chapter 5 we speculated that his difference might be resolved by including surface motion in our dynamics calculations because the experimental time-of-flight distributions are much broader compared to the theoretical ones[69].

It is clear that adding non-local correlation to the MS mGGA DFs has little effect on the $\nu = 1 : \nu = 0$ ratio of desorbing molecules. GGA based DFs yielded slightly better ratios for D_2 desorbing from Au(111)[15]. However, also these DFs predicted desorption ratios for H_2 that were much too low.

The fact that mGGA based DFs yield somewhat lower $\nu = 1 : \nu = 0$ ratios than the GGA based DFs[15] can be explained by the barriers to reaction predicted by the mGGA DFs being somewhat earlier. This allows the $\nu = 0$ population too grow somewhat relative to the $\nu = 1$ population, which would lower the $\nu = 1 : \nu = 0$ ratios.

6.3.5 Transferability

Previous work from our group has shown that semi-local DFs designed for the reaction of H_2 and D_2 dissociating on transition metals may be transferable

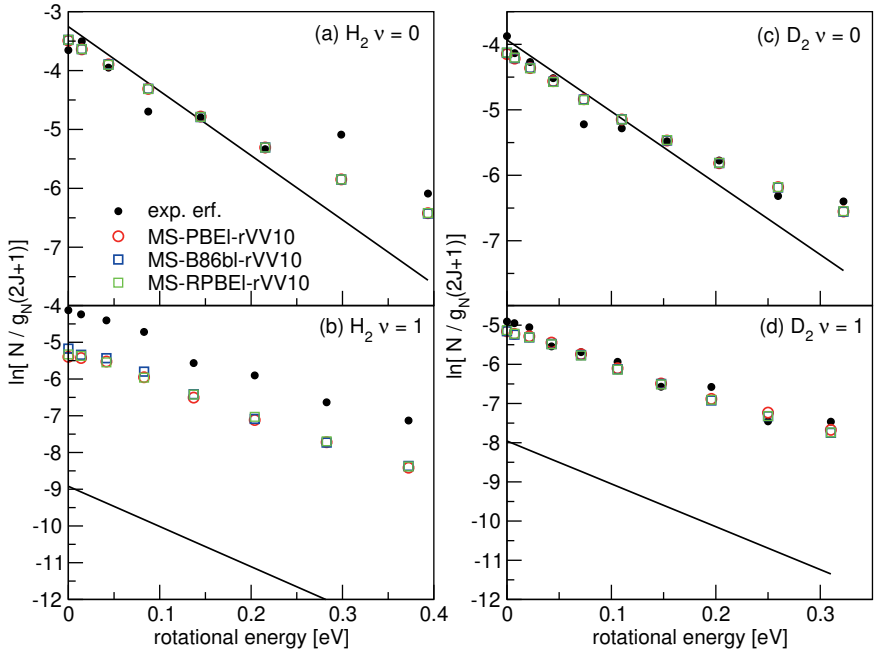

FIGURE 6.12: Rovibrational state populations of H_2 and D_2 desorbing from Au(111) are shown versus the rotational energy. Experimental results are shown in black[69], theoretical results are shown for MS-PBEl-rVV10 (red), MS-B86bl-rVV10 (blue) and MS-RPBEl-rVV10 (green) DF. The straight lines represent Boltzmann distributions for the surface temperature of the experiment.

between different crystal faces of the same metal[44,45], but until quite recently transferability between systems in which H_2 interacts with different metals had not yet been observed[64,138]. In Chapter 5 we have shown that non-local correlation is a key ingredient in obtaining SRP DFs for the reaction of H_2 and D_2 on transition metals that show this type of transferability, by showing that a DF that we designed to describe the activated reaction of H_2 + Cu(111) can also describe the reaction of D_2 + Pt(111) and vice versa[15]. Earlier, transferability of SRP-DFs between systems in which a molecule interacts with surfaces of different metals has only been reported for CH_4 reaction on Ni(111)[46] and CH_4 reacting on Pt(111)[47].

In our calculations we employ the BOSS model and thus neglect any surface temperature effects, and it is known that the BOSS model works well for activated H_2 dissociation on cold metals[20,50–52,54]. Given that associative desorption experiments necessitate high surface temperatures[69,72] it is difficult to asses the quality of the DFs we developed here for the H_2 (D_2) + Au(111) system, due to the absence of molecular beam sticking experiments for this system.

Here we show that the MS-PBEl-rVV10, MS-B86bl-rVV10 and MS-RPBEl-rVV10 DFs can describe molecular beam sticking experiments on D_2 + Ag(111) to within chemical accuracy (see figure 6.8), and that the MS-B86bl-rVV10 DF can also describe the D_2 + Pt(111) molecular beam sticking experiments of Luntz et al.[66] and Cao et al.[67] to within chemical accuracy (see figure 6.9). In the case of the H_2 (D_2) + Au(111) system the MS-PBEl-rVV10 DF yields very good results with respect to the calculated $E_{1/2}(\nu, J)$ parameters. To the best of our knowledge this is the first time that an observable of the reaction of H_2 (D_2) on Au(111) that requires dynamics calculations is described with chemical accuracy. However, uncertainties remain for this system with respect to the effects of surface temperature, surface reconstruction and ehp excitation[15].

Thus there now exist two groups of transferable (SRP) DFs for the reaction of H_2 (D_2) with transition metal surfaces. The first group consists of GGA based SRP DFs that use vdW-DF2[95] non-local correlation (B86SRP68-DF2[15] and PBEα57-DF2[14]), which can describe the H_2 (D_2) + Cu(111) and D_2 + Pt(111) reactions to within chemical accuracy. The second group consists of the MS mGGA DFs that use rVV10[48] non-local correlation developed here, which can describe the D_2 + Ag(111) and D_2 + Pt(111) systems with chemical accuracy. Of course there is also the non-conclusive evidence that suggests that the MS-PBEl-rVV10 DF can describe the associative desorption of H_2 from Au(111) to within chemical accuracy.

Presently we cannot say which features of a PES are most important, apart from the lowest barrier to reaction. Experiments that probe different parts of

a PES, like vibrationally or rotationally inelastic scattering, where the latter process depends on the anisotropy of the PES, are few and far between[139,140]. In general we see that the MS mGGA based DFs have somewhat earlier barriers for highly activated systems than the GGA based SRP DFs, while for the non-activated D_2 + Pt(111) system the barrier geometries of the MS mGGA based DFs that include rVV10[48] non-local correlation are very similar to the barrier geometries of GGA based SRP DFs that include vdW-DF2[95] non-local correlation. At the moment we cannot say which type of barrier geometry is more in line with reality.

If the suggested chemical accuracy in the description of H_2 + Au(111) holds in confrontation with experiment, then one could argue that the mGGA based DFs that include rVV10[48] non-local correlation are an improvement over the previously developed GGA based SRP DFs that include vdW-DF2[95] non-local correlation: in this case the MS mGGA-rVV10 based DFs can describe three systems with chemical accuracy, compared to two systems for the GGA based SRP DFs[15] developed in Chapter 5. This would indicate that climbing Jacob's ladder leads to a more universal description of the reaction of H_2 on transition metal surfaces.

6.4 Conclusion

We have combined our three previously developed MS-PBEl, MS-B86bl and MS-RPBEl mGGA DFs with rVV10 non-local correlation to obtain the MS-PBEl-rVV10, MS-B86bl-rVV10 and MS-RPBEl-rVV10 DFs. We find that all three developed DFs can describe the molecular beam sticking experiments on dissociative chemisorption of D_2 on Ag(111) with chemical accuracy. We also find that the the MS-B86bl-rVV10 DF can describe two sets of molecular beam sticking experiments on dissociative chemisorption of D_2 on Pt(111) with chemical accuracy. Additionally, by calculating $E_{1/2}(\nu, J)$ parameters for the reaction of H_2 on Au(111) and comparing these to experimental $E_0(\nu, J)$ parameters for state-selective associative desorption we obtain chemical accuracy with the MS-PBEl-rVV10 DF. Assessing the performance of the three developed MS mGGA-rVV10 DFs for the H_2 (D_2) + Au(111) system is however difficult due to the lack of well characterized molecular beam sticking experiments of H_2 (D_2) on Au(111) and the lack of calculations that use a reconstructed Au(111) surface and incorporate ehp excitation.

Of the three developed MS mGGA-rVV10 DFs, MS-PBEl-rVV10 performs excellently for the known van der Waals well geometries. The MS-PBEl-rVV10 DF also maintains the improvements generally observed for mGGA-rVV10

DFs relative to GGA-vdW-DF2 DFs in this regard. The MS-B86bl-rVV10 and MS-RPBEl-rVV10 DFs yield van der Waals wells that are too shallow.

In a comparisson to state-selected experiments on associative desorption of H_2 (D_2) from Ag(111) we observe excellent agreement with experiment in the case of H_2, for all three developed DFs. For H_2 all three developed DFs show improvement over the three original MS mGGA DFs and over the best GGA based SRP DFs that include vdW-DF2 non-local correlation. The associative desorption experiments on D_2 desorbing from Ag(111) were less well described.

With respect to the molecular beam sticking probabilities of H_2 (D_2) + Cu(111) the three developed DFs yield sticking probabilities in line with sticking probabilities predicted by the PBE DF, which are too high. This in contrast to the highly accurate sticking probabilities obtained when using the original three MS mGGA DFs.

The three original MS mGGA DFs give a description of the metal that is comparable to that obtained with the PBEsol DF. Unfortunately, adding rVV10 non-local correlation comes at the cost of a worse description of the metal. In general we see lattice constants that are smaller than the zero-point energy corrected experimental results. However, in general the underestimation of the calculated lattice constants is still smaller than the overestimation of calculated lattice constants obtained with the current best SRP DFs that include vdW-DF2 non-local correlation. The three developed MS mGGA-rVV10 DFs predict interlayer distances between the top two layers that are too large compared to experimental observations.

The three MS mGGA DFs that have been combined in this work with rVV10 non-local correlation were not fitted to reproduce particular experiments, nor has the b parameter present in rVV10 been re-optimized. Our results show that, overall, ascending Jacob's ladder from the GGA plus non-local correlation rung to the mGGA plus non-local correlation rung leads to somewhat more accurate results for dissociative chemisorption of H_2 (D_2) on noble metals, although the metals themselves are described less accurately than with the MS mGGA DFs without non-local van der Waals correlation, and the improvement does not hold for the well studied H_2 + Cu(111) system.

References

(1) Smeets, E. W. F.; Kroes, G.-J. Performance of made-simple meta-GGA functionals with rVV10 non-local correlation for H_2 + Cu(111), D_2 + Ag(111), H_2 + Au(111) and D_2 + Pt(111). *J. Phys. Chem. C* **2021**, DOI: 10.1021/acs.jpcc 0c11034.

(2) Wolcott, C. A.; Medford, A. J.; Studt, F.; Campbell, C. T. Degree of rate control approach to computational catalyst screening. *J. Catal.* **2015**, *330*, 197–207.

(3) Sabbe, M. K.; Reyniers, M.-F.; Reuter, K. First-principles kinetic modeling in heterogeneous catalysis: an industrial perspective on best-practice, gaps and needs. *Catal. Sci. Technol.* **2012**, *2*, 2010–2024.

(4) Ertl, G. Reactions at surfaces: from atoms to complexity (Nobel lecture). *Angew. Chem. Int. Ed.* **2008**, *47*, 3524–3535.

(5) Noyori, R. Synthesizing our future. *Nat. Chem.* **2009**, *1*, 5–6.

(6) Ertl, G. Primary steps in catalytic synthesis of ammonia. *J. Vac. Sci. Technol.* **1983**, *1*, 1247–1253.

(7) Waugh, K. Methanol synthesis. *Catal. Today* **1992**, *15*, 51–75.

(8) Grabow, L.; Mavrikakis, M. Mechanism of methanol synthesis on Cu through CO_2 and CO hydrogenation. *Acs Catalysis* **2011**, *1*, 365–384.

(9) Behrens, M.; Studt, F.; Kasatkin, I.; Kühl, S.; Hävecker, M.; Abild-Pedersen, F.; Zander, S.; Girgsdies, F.; Kurr, P.; Kniep, B.-L., et al. The active site of methanol synthesis over $Cu/ZnO/Al_2O_3$ industrial catalysts. *Science* **2012**, *336*, 893–897.

(10) Kroes, G.-J. Toward a database of chemically accurate barrier heights for reactions of molecules with metal surfaces. *J. Phys. Chem lett.* **2015**, *6*, 4106–4114.

(11) Stegelmann, C.; Andreasen, A.; Campbell, C. T. Degree of rate control: how much the energies of intermediates and transition states control rates. *J. Am. Chem. Soc.* **2009**, *131*, 8077–8082.

(12) Park, G. B.; Kitsopoulos, T. N.; Borodin, D.; Golibrzuch, K.; Neugebohren, J.; Auerbach, D. J.; Campbell, C. T.; Wodtke, A. M. The kinetics of elementary thermal reactions in heterogeneous catalysis. *Nature Rev. Chem.* **2019**, *3*, 723–732.

(13) Díaz, C.; Pijper, E.; Olsen, R.; Busnengo, H.; Auerbach, D.; Kroes, G. Chemically accurate simulation of a prototypical surface reaction: H_2 dissociation on Cu(111). *Science* **2009**, *326*, 832–834.

(14) Ghassemi, E. N.; Wijzenbroek, M.; Somers, M. F.; Kroes, G.-J. Chemically accurate simulation of dissociative chemisorption of D_2 on Pt(111). *Chem. Phys. Lett.* **2017**, *683*, 329–335.

(15) Smeets, E. W. F.; Kroes, G.-J. Designing new SRP density functionals including non-local vdW-DF2 correlation for H_2 + Cu(111) and their transferability to H_2 + Ag(111), Au(111) and Pt(111). *Phys. Chem. Chem. Phys.* **2021**, *23*, 7875–7901.

(16) Gerrits, N.; Smeets, E. W. F.; Vuckovic, S.; Powell, A. D.; Doblhoff-Dier, K.; Kroes, G.-J. Density functional theory for molecule–metal surface reactions: When does the generalized gradient approximation get it right, and what to do if it does not. *J. Phys. Chem. Lett,* **2020**, *11*, 10552–10560.

(17) Schimka, L.; Harl, J.; Stroppa, A.; Grüneis, A.; Marsman, M.; Mittendorfer, F.; Kresse, G. Accurate surface and adsorption energies from many-body perturbation theory. *Nature materials* **2010**, *9*, 741–744.

(18) Haas, P.; Tran, F.; Blaha, P.; Schwarz, K. Construction of an optimal GGA functional for molecules and solids. *Phys. Rev. B* **2011**, *83*, 205117.

(19) Peverati, R.; Truhlar, D. G. Exchange–correlation functional with good accuracy for both structural and energetic properties while depending only on the density and its gradient. *J. Chem. Theory Comput.* **2012**, *8*, 2310–2319.

(20) Nattino, F.; Díaz, C.; Jackson, B.; Kroes, G.-J. Effect of surface motion on the rotational quadrupole alignment parameter of D_2 reacting on Cu(111). *Phys. Rev. Lett.* **2012**, *108*, 236104.

(21) Marashdeh, A.; Casolo, S.; Sementa, L.; Zacharias, H.; Kroes, G.-J. Surface temperature effects on dissociative chemisorption of H_2 on Cu(100). *J. Phys. Chem. C* **2013**, *117*, 8851–8863.

(22) Mondal, A.; Wijzenbroek, M.; Bonfanti, M.; Díaz, C.; Kroes, G.-J. Thermal lattice expansion effect on reactive scattering of H_2 from Cu(111) at T_s = 925 K. *J. Phys. Chem. A* **2013**, *117*, 8770–8781.

(23) Tiwari, A. K.; Nave, S.; Jackson, B. Methane dissociation on Ni(111): A new understanding of the lattice effect. *Phys. Rev. Lett.* **2009**, *103*, 253201.

(24) Tiwari, A. K.; Nave, S.; Jackson, B. The temperature dependence of methane dissociation on Ni(111) and Pt(111): mixed quantum-classical studies of the lattice response. *J. Chem. Phys.* **2010**, *132*, 134702.

(25) Smeets, E. W. F.; Voss, J.; Kroes, G.-J. Specific reaction parameter density functional based on the meta-generalized gradient approximation: application to H_2 + Cu(111) and H_2 + Ag(111). *J. Phys. Chem. A* **2019**, *123*, 5395–5406.

(26) Sun, J.; Xiao, B.; Ruzsinszky, A. Communication: Effect of the orbital-overlap dependence in the meta generalized gradient approximation. *J. Chem. Phys.* **2012**, *137*, 051101.

(27) Sun, J.; Haunschild, R.; Xiao, B.; Bulik, I. W.; Scuseria, G. E.; Perdew, J. P. Semilocal and hybrid meta-generalized gradient approximations based on the understanding of the kinetic-energy-density dependence. *J. Chem. Phys.* **2013**, *138*, 044113.

(28) Perdew, J. P.; Ruzsinszky, A.; Csonka, G. I.; Vydrov, O. A.; Scuseria, G. E.; Constantin, L. A.; Zhou, X.; Burke, K. Restoring the density-gradient expansion for exchange in solids and surfaces. *Phys. Rev. Lett.* **2008**, *100*, 136406.

(29) Michelsen, H.; Rettner, C.; Auerbach, D.; Zare, R. Effect of rotation on the translational and vibrational energy dependence of the dissociative adsorption of D_2 on Cu(111). *J. Chem. Phys.* **1993**, *98*, 8294–8307.

(30) Berger, H.; Leisch, M.; Winkler, A.; Rendulic, K. A search for vibrational contributions to the activated adsorption of H_2 on copper. *Chem. Phys. Lett.* **1990**, *175*, 425–428.

(31) Rettner, C.; Michelsen, H.; Auerbach, D. Quantum-state-specific dynamics of the dissociative adsorption and associative desorption of H_2 at a Cu(111) surface. *J. Chem. Phys.* **1995**, *102*, 4625–4641.

(32) Cottrell, C.; Carter, R.; Nesbitt, A.; Samson, P.; Hodgson, A. Vibrational state dependence of D_2 dissociation on Ag(111). *J. Chem. Phys.* **1997**, *106*, 4714–4722.

(33) Sun, J.; Xiao, B.; Fang, Y.; Haunschild, R.; Hao, P.; Ruzsinszky, A.; Csonka, G. I.; Scuseria, G. E.; Perdew, J. P. Density functionals that recognize covalent, metallic, and weak bonds. *Phys. Rev. Lett.* **2013**, *111*, 106401.

(34) Tao, J.; Perdew, J. P.; Staroverov, V. N.; Scuseria, G. E. Climbing the density functional ladder: Nonempirical meta-generalized gradient approximation designed for molecules and solids. *Phys. Rev. Lett.* **2003**, *91*, 146401.

(35) Perdew, J. P.; Ruzsinszky, A.; Csonka, G. I.; Constantin, L. A.; Sun, J. Workhorse semilocal density functional for condensed matter physics and quantum chemistry. *Phys. Rev. Lett.* **2009**, *103*, 026403.

(36) Garza, A. J.; Bell, A. T.; Head-Gordon, M. Nonempirical meta-generalized gradient approximations for modeling chemisorption at metal surfaces. *J. Chem. Theory Comput.* **2018**, *14*, 3083–3090.

(37) Sun, J.; Ruzsinszky, A.; Perdew, J. P. Strongly constrained and appropriately normed semilocal density functional. *Phys. Rev. Lett.* **2015**, *115*, 036402.

(38) Peng, H.; Yang, Z.-H.; Perdew, J. P.; Sun, J. Versatile van der Waals density functional based on a meta-generalized gradient approximation. *Phys. Rev. X* **2016**, *6*, 041005.

(39) Wellendorff, J.; Lundgaard, K. T.; Jacobsen, K. W.; Bligaard, T. mBEEF: An accurate semi-local Bayesian error estimation density functional. *J. Chem. Phys.* **2014**, *140*, 144107.

(40) Lundgaard, K. T.; Wellendorff, J.; Voss, J.; Jacobsen, K. W.; Bligaard, T. mBEEF-vdW: Robust fitting of error estimation density functionals. *Phys. Rev. B* **2016**, *93*, 235162.

(41) Sun, J.; Marsman, M.; Ruzsinszky, A.; Kresse, G.; Perdew, J. P. Improved lattice constants, surface energies, and CO desorption energies from a semilocal density functional. *Phys. Rev. B* **2011**, *83*, 121410.

(42) Sun, J.; Perdew, J. P.; Ruzsinszky, A. Semilocal density functional obeying a strongly tightened bound for exchange. *Proc. Nat. Ac. Sci.* **2015**, *112*, 685–689.

(43) Peverati, R.; Truhlar, D. G. An improved and broadly accurate local approximation to the exchange-correlation density functional: The MN12-L functional for electronic structure calculations in chemistry and physics. *Phys. Chem. Chem. Phys.* **2012**, *14*, 13171–13174.

(44) Ghassemi, E. N.; Smeets, E. W. F.; Somers, M. F.; Kroes, G.-J.; Groot, I. M.; Juurlink, L. B.; Füchsel, G. Transferability of the specific reaction parameter density functional for H_2 + Pt(111) to H_2 + Pt(211). *J. Phys. Chem. C* **2019**, *123*, 2973–2986.

(45) Sementa, L.; Wijzenbroek, M.; Van Kolck, B.; Somers, M.; Al-Halabi, A.; Busnengo, H. F.; Olsen, R.; Kroes, G.-J.; Rutkowski, M.; Thewes, C., et al. Reactive scattering of H_2 from Cu(100): comparison of dynamics calculations based on the specific reaction parameter approach to density functional theory with experiment. *J. Chem. Phys.* **2013**, *138*, 044708.

(46) Nattino, F.; Migliorini, D.; Kroes, G.-J.; Dombrowski, E.; High, E. A.; Killelea, D. R.; Utz, A. L. Chemically accurate simulation of a polyatomic molecule-metal surface reaction. *J. Phys. Chem. Lett.* **2016**, *7*, 2402–2406.

(47) Migliorini, D.; Chadwick, H.; Nattino, F.; Gutiérrez-González, A.; Dombrowski, E.; High, E. A.; Guo, H.; Utz, A. L.; Jackson, B.; Beck, R. D., et al. Surface reaction barriometry: methane dissociation on flat and stepped transition-metal surfaces. *J. Phys. Chem. Lett.* **2017**, *8*, 4177–4182.

(48) Sabatini, R.; Gorni, T.; De Gironcoli, S. Nonlocal van der Waals density functional made simple and efficient. *Phys. Rev. B* **2013**, *87*, 041108.

(49) Vydrov, O. A.; Van Voorhis, T. Nonlocal van der Waals density functional: The simpler the better. *J. Chem. Phys.* **2010**, *133*, 244103.

(50) Díaz, C.; Olsen, R. A.; Auerbach, D. J.; Kroes, G.-J. Six-dimensional dynamics study of reactive and non reactive scattering of H_2 from Cu(111) using a chemically accurate potential energy surface. *Phys. Chem. Chem. Phys.* **2010**, *12*, 6499–519.

(51) Wijzenbroek, M.; Somers, M. F. Static surface temperature effects on the dissociation of H_2 and D_2 on Cu(111). *J. Chem. Phys.* **2012**, *137*, 054703.

(52) Spiering, P.; Wijzenbroek, M.; Somers, M. An improved static corrugation model. *J. Chem. Phys.* **2018**, *149*, 234702.

(53) Nattino, F.; Genova, A.; Guijt, M.; Muzas, A. S.; Díaz, C.; Auerbach, D. J.; Kroes, G.-J. Dissociation and recombination of D_2 on Cu(111): Ab initio molecular dynamics calculations and improved analysis of desorption experiments. *J. Chem. Phys.* **2014**, *141*, 124705.

(54) Kroes, G.-J.; Díaz, C. Quantum and classical dynamics of reactive scattering of H_2 from metal surfaces. *Chem. Soc. Rev.* **2016**, *45*, 3658–3700.

(55) Bonfanti, M.; Somers, M. F.; Díaz, C.; Busnengo, H. F.; Kroes, G.-J. 7D quantum dynamics of H_2 scattering from Cu(111): the accuracy of the phonon sudden approximation. *Z. Phys. Chem.* **2013**, *227*, 1397–1420.

(56) Spiering, P.; Meyer, J. Testing electronic friction models: vibrational de-excitation in scattering of H_2 and D_2 from Cu(111). *J. Phys. Chem. Lett.* **2018**, *9*, 1803–1808.

(57) Muzas, A. S.; Juaristi, J. I.; Alducin, M.; Díez Muiño, R.; Kroes, G.-J.; Díaz, C. Vibrational deexcitation and rotational excitation of H_2 and D_2 scattered from Cu(111): adiabatic versus non-adiabatic dynamics. *J. Chem. Phys.* **2012**, *137*, 064707.

(58) Luntz, A. C.; Persson, M. How adiabatic is activated adsorption/associative desorption? *The Journal of chemical physics* **2005**, *123*, 074704.

(59) Maurer, R. J.; Zhang, Y.; Guo, H.; Jiang, B. Hot electron effects during reactive scattering of H_2 from Ag(111): assessing the sensitivity to initial conditions, coupling magnitude, and electronic temperature. *Faraday Discuss.* **2019**, *214*, 105–121.

(60) Zhang, Y.; Maurer, R. J.; Guo, H.; Jiang, B. Hot-electron effects during reactive scattering of H_2 from Ag(111): the interplay between mode-specific electronic friction and the potential energy landscape. *Chem. Sci.* **2019**, *10*, 1089–1097.

(61) Maurer, R. J.; Jiang, B.; Guo, H.; Tully, J. C. Mode specific electronic friction in dissociative chemisorption on metal surfaces: H 2 on Ag (111). *Physical review letters* **2017**, *118*, 256001.

(62) Füchsel, G.; Schimka, S.; Saalfrank, P. On the role of electronic friction for dissociative adsorption and scattering of hydrogen molecules at a Ru(0001) surface. *J. Phys. Chem. A* **2013**, *117*, 8761–8769.

(63) Füchsel, G.; Cao, K.; Er, S.; Smeets, E. W. F.; Kleyn, A. W.; Juurlink, L. B. F.; Kroes, G.-J. Anomalous dependence of the reactivity on the presence of steps: dissociation of D_2 on Cu(211). *J. Phys. Chem. Lett.* **2018**, *9*, 170–175.

(64) Nour Ghassemi, E.; Somers, M.; Kroes, G.-J. Test of the transferability of the specific reaction parameter functional for H_2+ Cu(111) to D_2 + Ag(111). *J. Phys. Chem. C* **2018**, *122*, 22939–22952.

(65) Crespos, C.; Collins, M. A.; Pijper, E.; Kroes, G.-J. Multi-dimensional potential energy surface determination by modified Shepard interpolation for a molecule–surface reaction: H_2 + Pt(111). *Chem. Phys. Lett.* **2003**, *376*, 566–575.

(66) Luntz, A.; Brown, J.; Williams, M. Molecular beam studies of H_2 and D_2 dissociative chemisorption on Pt(111). *J. Chem. Phys.* **1990**, *93*, 5240–5246.

(67) Cao, K.; Füchsel, G.; Kleyn, A. W.; Juurlink, L. B. Hydrogen adsorption and desorption from Cu(111) and Cu(211). *Phys. Chem. Chem. Phys.* **2018**, *20*, 22477–22488.

(68) Samson, P.; Nesbitt, A.; Koel, B. E.; Hodgson, A. Deuterium dissociation on ordered Sn/Pt(111) surface alloys. *J. Chem. Phys.* **1998**, *109*, 3255–3264.

(69) Shuai, Q.; Kaufmann, S.; Auerbach, D. J.; Schwarzer, D.; Wodtke, A. M. Evidence for electron–hole pair excitation in the associative desorption of H_2 and D_2 from Au(111). *J. Phys. Chem. Lett.* **2017**, *8*, 1657–1663.

(70) Murphy, M.; Hodgson, A. Translational energy release in the recombinative desorption of H_2 from Ag(111). *Surf. Sci.* **1997**, *390*, 29–34.

(71) Murphy, M.; Hodgson, A. Role of surface thermal motion in the dissociative chemisorption and recombinative desorption of D_2 on Ag(111). *Phys. Rev. Lett.* **1997**, *78*, 4458–4461.

(72) Kaufmann, S.; Shuai, Q.; Auerbach, D. J.; Schwarzer, D.; Wodtke, A. M. Associative desorption of hydrogen isotopologues from copper surfaces: characterization of two reaction mechanisms. *J. Chem. Phys.* **2018**, *148*, 194703.

(73) Perrier, A.; Bonnet, L.; Liotard, D.; Rayez, J.-C. On the dynamics of H_2 desorbing from a Pt(111) surface. *Surf. Sci.* **2005**, *581*, 189–198.

(74) Perrier, A.; Bonnet, L.; Rayez, J.-C. Dynamical study of H_2 and D_2 desorbing from a Cu(111) surface. *J. Phys. Chem. A* **2006**, *110*, 1608–1617.

(75) Perrier, A.; Bonnet, L.; Rayez, J.-C. Statisticodynamical approach of final state distributions in associative desorptions. *J. Chem. Phys.* **2006**, *124*, 194701.

(76) Díaz, C.; Perrier, A.; Kroes, G. Associative desorption of N_2 from Ru(0001): a computational study. *Chem. Phys. Lett.* **2007**, *434*, 231–236.

(77) Galparsoro, O.; Kaufmann, S.; Auerbach, D. J.; Kandratsenka, A.; Wodtke, A. M. First principles rates for surface chemistry employing exact transition state theory: application to recombinative desorption of hydrogen from Cu(111). *Phys. Chem. Chem. Phys.* **2020**, *22*, 17532–17539.

(78) Dai, J.; Zhang, J. Z. Quantum adsorption dynamics of a diatomic molecule on surface: four-dimensional fixed-site model for H_2 on Cu(111). *J. Chem. Phys.* **1995**, *102*, 6280–6289.

(79) Hammer, B.; Scheffler, M.; Jacobsen, K. W.; Nørskov, J. K. Multidimensional potential energy surface for H_2 dissociation over Cu(111). *Phys. Rev. Lett.* **1994**, *73*, 1400–1403.

(80) Cowin, J. P.; Yu, C.-F.; Sibener, S. J.; Hurst, J. E. Bound level resonances in rotationally inelastic HD/Pt (111) surface scattering. *The Journal of Chemical Physics* **1981**, *75*, 1033–1034.

(81) Cowin, J. P.; Yu, C.-F.; Sibener, S. J.; Wharton, L. HD scattering from Pt(111): rotational excitation probabilities. *J. Chem. Phys.* **1983**, *79*, 3537–3549.

(82) Cowin, J. P.; Yu, C.-F.; Wharton, L. HD scattering from Pt(111): Rotationally mediated selective adsorption. *Surf. Sci.* **1985**, *161*, 221–233.

(83) Yu, C.-F.; Hogg, C. S.; Cowin, J. P.; Whaley, K. B.; Light, J. C.; Sibener, S. J. Rotationally mediated selective adsorption as a probe of isotropic and anisotropic molecule—surface interaction potentials: HD (J)/Ag(111). *Israel J. Chem.* **1982**, *22*, 305–314.

(84) Yu, C.-f.; Whaley, K. B.; Hogg, C. S.; Sibener, S. J. Investigation of the spatially isotropic component of the laterally averaged molecular hydrogen/Ag(111) physisorption potential. *J. Chem. Phys.* **1985**, *83*, 4217–4234.

(85) Perreau, J.; Lapujoulade, J. Selective adsorption of He, H_2 on copper surfaces. *Surf. Sci.* **1982**, *122*, 341–354.

(86) Yu, C.-f.; Whaley, K. B.; Hogg, C. S.; Sibener, S. J. Selective Adsorption Resonances in the Scattering of n-H_2 p-H_2 n-D_2 and o-D_2 from Ag(111). *Phys. Rev. Lett.* **1983**, *51*, 2210.

(87) Kaufhold, A.; Toennies, J. P. An optical potential for rotationally mediated selective adsorption (Feshbach) resonances in scattering of molecules from smooth crystal surfaces. *Surf. Sci.* **1986**, *173*, 320–336.

(88) Andersson, S.; Wilzén, L.; Persson, M. Physisorption interaction of H_2 with noble-metal surfaces: A new H_2-Cu potential. *Phys. Rev. B* **1988**, *38*, 2967.

(89) Andersson, S.; Persson, M. Sticking in the physisorption well: influence of surface structure. *Phys. Rev. Lett.* **1993**, *70*, 202.

(90) Harten, U.; Toennies, J. P.; Wöll, C. Molecular beam translational spectroscopy of physisorption bound states of molecules on metal surfaces. I. HD on Cu(111) and Au(111) single crystal surfaces. *J. Chem. Phys.* **1986**, *85*, 2249–2258.

(91) Lennard-Jones, J. E.; Devonshire, A. F. Diffraction and selective adsorption of atoms at crystal surfaces. *Nature* **1936**, *137*, 1069–1070.

(92) Hoinkes, H.; Wilsch, H. In *Helium Atom Scattering from Surfaces*; Springer: 1992, pp 113–172.

(93) Poelsema, B.; Lenz, K.; Comsa, G. The dissociative adsorption of hydrogen on defect-free Pt(111). *J. Phys. Condens. Matter* **2010**, *22*, 304006.

(94) Dion, M.; Rydberg, H.; Schröder, E.; Langreth, D. C.; Lundqvist, B. I. Van der Waals density functional for general geometries. *Phys. Rev. Lett.* **2004**, *92*, 246401.

(95) Lee, K.; Murray, É. D.; Kong, L.; Lundqvist, B. I.; Langreth, D. C. Higher-accuracy van der Waals density functional. *Phys. Rev. B* **2010**, *82*, 081101.

(96) Mardirossian, N.; Head-Gordon, M. Thirty years of density functional theory in computational chemistry: an overview and extensive assessment of 200 density functionals. *Mol. Phys.* **2017**, *115*, 2315–2372.

(97) Mardirossian, N.; Ruiz Pestana, L.; Womack, J. C.; Skylaris, C.-K.; Head-Gordon, T.; Head-Gordon, M. Use of the rVV10 nonlocal correlation functional in the B97M-V density functional: Defining B97M-rV and related functionals. *J. Phys. Chem. Lett.* **2017**, *8*, 35–40.

(98) Murray, É. D.; Lee, K.; Langreth, D. C. Investigation of exchange energy density functional accuracy for interacting molecules. *J. Chem. Theor. Comput.* **2009**, *5*, 2754–2762.

(99) Perdew, J. P.; Burke, K.; Ernzerhof, M. Generalized gradient approximation made simple. *Phys. Rev. Lett.* **1996**, *77*, 3865–3868.

(100) Giannozzi, P.; Baroni, S.; Bonini, N.; Calandra, M.; Car, R.; Cavazzoni, C.; Ceresoli, D.; Chiarotti, G. L.; Cococcioni, M.; Dabo, I., et al. QUANTUM ESPRESSO: a modular and open-source software project for quantum simulations of materials. *J. Phys. Condens. Matt.* **2009**, *21*, 395502.

(101) Giannozzi, P.; Andreussi, O.; Brumme, T.; Bunau, O.; Nardelli, M. B.; Calandra, M.; Car, R.; Cavazzoni, C.; Ceresoli, D.; Cococcioni, M., et al. Advanced capabilities for materials modelling with Quantum ESPRESSO. *J. Phys. Condens. Matt.* **2017**, *29*, 465901.

(102) Shao, Y.; Gan, Z.; Epifanovsky, E.; Gilbert, A. T.; Wormit, M.; Kussmann, J.; Lange, A. W.; Behn, A.; Deng, J.; Feng, X., et al. Advances in molecular quantum chemistry contained in the Q-Chem 4 program package. *Mol. Phys.* **2015**, *113*, 184–215.

(103) Román-Pérez, G.; Soler, J. M. Efficient implementation of a van der Waals density functional: application to double-wall carbon nanotubes. *Phys. Rev. Lett.* **2009**, *103*, 096102.

(104) Perdew, J. P.; Wang, Y. Pair-distribution function and its coupling-constant average for the spin-polarized electron gas. *Phys. Rev. B* **1992**, *46*, 12947.

(105) Jurečka, P.; Šponer, J.; Černy, J.; Hobza, P. Benchmark database of accurate (MP2 and CCSD (T) complete basis set limit) interaction energies of small model complexes, DNA base pairs, and amino acid pairs. *Phys. Chem. Chem. Phys.* **2006**, *8*, 1985–1993.

(106) Hammer, B. H. L. B.; Hansen, L. B.; Nørskov, J. K. Improved adsorption energetics within density-functional theory using revised Perdew-Burke-Ernzerhof functionals. *Phys. Rev. B* **1999**, *59*, 7413–7421.

(107) Becke, A. D. On the large-gradient behavior of the density functional exchange energy. *J. Chem. Phys.* **1986**, *85*, 7184–7187.

(108) Haas, P.; Tran, F.; Blaha, P. Calculation of the lattice constant of solids with semilocal functionals. *Phys. Rev. B* **2009**, *79*, 085104.

(109) Busnengo, H.; Salin, A.; Dong, W. Representation of the 6D potential energy surface for a diatomic molecule near a solid surface. *J. Chem. Phys.* **2000**, *112*, 7641–7651.

(110) Wijzenbroek, M.; Klein, D. M.; Smits, B.; Somers, M. F.; Kroes, G.-J. Performance of a non-local van der Waals density functional on the dissociation of H_2 on metal surfaces. *J. Phys. Chem. A* **2015**, *119*, 12146–12158.

(111) Raff, L. M.; Karplus, M. Theoretical investigations of reactive collisions in molecular beams: K+CH_3I and related systems. *J. Chem. Phys.* **1966**, *44*, 1212–1229.

(112) Stoer, J.; Bulirsch, R., *Introduction to numerical analysis*; Springer Science & Business Media, New York: 2013; Vol. 12.

(113) Füchsel, G.; del Cueto, M.; Díaz, C.; Kroes, G.-J. Enigmatic HCl + Au(111) reaction: a puzzle for theory and experiment. *J. Phys. Chem. C* **2016**, *120*, 25760–25779.

(114) Kaufmann, S. personal communication.

(115) Kresse, G.; Hafner, J. Ab initio molecular-dynamics simulation of the liquid-metal–amorphous-semiconductor transition in germanium. *Phys. Rev. B* **1994**, *49*, 14251–14269.

(116) Kresse, G.; Hafner, J. Ab initio molecular dynamics for liquid metals. *Phys. Rev. B* **1993**, *47*, 558–561.

(117) Kresse, G.; Furthmüller, J. Efficient iterative schemes for ab initio total-energy calculations using a plane-wave basis set. *Phys. Rev. B* **1996**, *54*, 11169–11186.

(118) Kresse, G.; Furthmüller, J. Efficiency of ab-initio total energy calculations for metals and semiconductors using a plane-wave basis set. *Comput. Mater. Sci.* **1996**, *6*, 15–50.

(119) Blöchl, P. E. Projector augmented-wave method. *Phys. Rev. B* **1994**, *50*, 17953–17979.

(120) Klimeš, J. ř.; Bowler, D. R.; Michaelides, A. Van der Waals density functionals applied to solids. *Phys. Rev. B* **2011**, *83*, 195131.

(121) Román-Pérez, G.; Soler, J. M. Efficient implementation of a Van der Waals density functional: application to double-wall carbon nanotubes. *Phys. Rev. Lett.* **2009**, *103*, 096102.

(122) Klimeš, J.; Bowler, D. R.; Michaelides, A. Chemical accuracy for the van der Waals density functional. *J. Phys. Condens. Matter* **2009**, *22*, 022201.

(123) Chae, K.; Lu, H.; Gustafsson, T. Medium-energy ion-scattering study of the temperature dependence of the structure of Cu(111). *Phys. Rev. B* **1996**, *54*, 14082.

(124) Okazawa, T.; Takeuchi, F.; Kido, Y. Enhanced and correlated thermal vibrations of Cu(111) and Ni(111) surfaces. *Physical Review B* **2005**, *72*, 075408.

(125) Lindgren, S.; Walldén, L.; Rundgren, J.; Westrin, P. Low-energy electron diffraction from Cu(111): subthreshold effect and energy-dependent inner potential; surface relaxation and metric distances between spectra. *Phys. Rev. B* **1984**, *29*, 576–588.

(126) Statiris, P.; Lu, H.; Gustafsson, T. Temperature dependent sign reversal of the surface contraction of Ag(111). *Phys. Rev. Lett.* **1994**, *72*, 3574–3577.

(127) Soares, E.; Leatherman, G.; Diehl, R.; Van Hove, M. Low-energy electron diffraction study of the thermal expansion of Ag(111). *Surf. Sci.* **2000**, *468*, 129–136.

(128) Nichols, R.; Nouar, T.; Lucas, C.; Haiss, W.; Hofer, W. Surface relaxation and surface stress of Au(111). *Surf. Sci.* **2002**, *513*, 263–271.

(129) Adams, D. L.; Nielsen, H.; Van Hove, M. A. Quantitative analysis of low-energy-electron diffraction: application to Pt(111). *Phys. Rev. B* **1979**, *20*, 4789.

(130) Lee, K.; Berland, K.; Yoon, M.; Andersson, S.; Schröder, E.; Hyldgaard, P.; Lundqvist, B. I. Benchmarking van der Waals density functionals with experimental data: potential-energy curves for H_2 molecules on Cu(111),(100) and (110) surfaces. *J. Phys. Condens. Matter* **2012**, *24*, 424213.

(131) Kroes, G.-J. Frontiers in surface scattering simulations. *Science* **2008**, *321*, 794–797.

(132) Ghassemi, E. N.; Somers, M. F.; Kroes, G.-J. Assessment of two problems of specific reaction parameter density functional theory: sticking and diffraction of H_2 on Pt(111). *J. Phys. Chem. C* **2019**, *123*, 10406–10418.

(133) Wijzenbroek, M.; Helstone, D.; Meyer, J.; Kroes, G.-J. Dynamics of H_2 dissociation on the close-packed (111) surface of the noblest metal: H_2 + Au(111). *J. Chem. Phys.* **2016**, *145*, 144701.

(134) Mukherjee, S.; Libisch, F.; Large, N.; Neumann, O.; Brown, L. V.; Cheng, J.; Lassiter, J. B.; Carter, E. A.; Nordlander, P.; Halas, N. J. Hot electrons do the impossible: plasmon-induced dissociation of H_2 on Au. *Nano lett.* **2012**, *13*, 240–247.

(135) Hasselbrink, E. Non-adiabaticity in surface chemical reactions. *Surf. Sci.* **2009**, *603*, 1564–1570.

(136) Schindler, B.; Diesing, D.; Hasselbrink, E. Electronic excitations induced by hydrogen surface chemical reactions on gold. *J. Chem. Phys.* **2011**, *134*, 034705.

(137) Schindler, B.; Diesing, D.; Hasselbrink, E. Electronically nonadiabatic processes in the interaction of H with a Au surface revealed using MIM junctions: the temperature dependence. *J. Phys. Chem. C* **2013**, *117*, 6337–6345.

(138) Tchakoua, T.; Smeets, E. W. F.; Somers, M.; Kroes, G.-J. Toward a specific reaction parameter density functional for H_2 + Ni(111): comparison of theory with molecular beam sticking experiments. *J. Phys. Chem. C* **2019**, *123*, 20420–20433.

(139) Hou, H.; Gulding, S.; Rettner, C.; Wodtke, A.; Auerbach, D. The stereodynamics of a gas-surface reaction. *Science* **1997**, *277*, 80–82.

(140) Hodgson, A.; Samson, P.; Wight, A.; Cottrell, C. Rotational excitation and vibrational relaxation of H_2 (ν= 1, J= 0) Scattered from Cu(111). *Phys. Rev. Lett.* **1997**, *78*, 963–966.